

First Search for Heavy Neutral Leptons with IceCube DeepCore

Dissertation

zur Erlangung des akademischen Grades
doctor rerum naturalium
(Dr. rer. nat.)

im Fach: Physik
Spezialisierung: Experimentalphysik

eingereicht an der
Mathematisch-Naturwissenschaftlichen Fakultät
der Humboldt-Universität zu Berlin

von

Leander Fischer M. Sc.
geboren am 24. Oktober 1992
in Heidelberg

Präsidentin der Humboldt-Universität zu Berlin
Prof. Dr. Julia von Blumenthal

Dekanin der Mathematisch-Naturwissenschaftlichen Fakultät
Prof. Dr. Caren Tischendorf

Copyright Notice

This book is released into the public domain using the CC-BY-4.0 code.

To view a copy of the CC-BY-4.0 code, visit:

<https://creativecommons.org/licenses/by/4.0/>

Colophon

This document was typeset with the help of KOMA-Script and L^AT_EX using the open-source kaobook template class.

The source code of this thesis is available at:

https://github.com/LeanderFischer/phd_thesis

Foreword

Before diving into the scientific content of my work, I would like to give some editorial remarks to smoothen the reading experience. Throughout the thesis, acronyms and experiment names are introduced in *italic font*, the first time they are mentioned, but are used in normal font from then on. The same goes for software packages, which are initially mentioned in SMALL CAPS FONT. One of the key features of the kaobok template - the big margin - is put to good use to house tables, figures, and additional notes, but also to highlight selected references. Of course, all references are listed in their full extent in the bibliography at the end, but additionally, some (but not necessarily all) of them will be highlighted in the margin next to where they appear to allow for an uninterrupted flow of reading.

Abstract

The observation of neutrino oscillations has established that neutrinos have non-zero masses. This phenomenon is not explained by the *standard model (SM)* of particle physics, but one viable explanation to this dilemma is the existence of *heavy neutral leptons (HNLs)* in the form of right-handed neutrinos. Depending on their mass and coupling to SM neutrinos, these particles could also play an important role in solving additional unexplained observations such as *dark matter (DM)* and the *baryon asymmetry of the universe (BAU)*. This work presents the first search for HNLs with the IceCube Neutrino Observatory. The standard three flavor neutrino model is extended by adding a fourth GeV-scale mass state and allowing mixing with the tau neutrino through the mixing parameter $|U_{\tau 4}|^2$. Three HNL mass values, m_4 , of 0.3 GeV, 0.6 GeV, and 1.0 GeV are tested using ten years of data, collected between 2011 and 2021, resulting in constraints for the mixing parameter of $|U_{\tau 4}|^2 < 0.19$ ($m_4 = 0.3$ GeV), $|U_{\tau 4}|^2 < 0.36$ ($m_4 = 0.6$ GeV), and $|U_{\tau 4}|^2 < 0.40$ ($m_4 = 1.0$ GeV) at 90 % confidence level. No significant signal of HNLs is observed for any of the tested masses. This first analysis lays the fundamental groundwork for future searches for HNLs in IceCube.

Zusammenfassung

The observation of neutrino oscillations has established that neutrinos have non-zero masses. This phenomenon is not explained by the *standard model (SM)* of particle physics, but one viable explanation to this dilemma is the existence of *heavy neutral leptons (HNLs)* in the form of right-handed neutrinos. Depending on their mass and coupling to SM neutrinos, these particles could also play an important role in solving additional unexplained observations such as *dark matter (DM)* and the *baryon asymmetry of the universe (BAU)*. This work presents the first search for HNLs with the IceCube Neutrino Observatory. The standard three flavor neutrino model is extended by adding a fourth GeV-scale mass state and allowing mixing with the tau neutrino through the mixing parameter $|U_{\tau 4}|^2$. Three HNL mass values, m_4 , of 0.3 GeV, 0.6 GeV, and 1.0 GeV are tested using ten years of data, collected between 2011 and 2021, resulting in constraints for the mixing parameter of $|U_{\tau 4}|^2 < 0.19$ ($m_4 = 0.3$ GeV), $|U_{\tau 4}|^2 < 0.36$ ($m_4 = 0.6$ GeV), and $|U_{\tau 4}|^2 < 0.40$ ($m_4 = 1.0$ GeV) at 90 % confidence level. No significant signal of HNLs is observed for any of the tested masses. This first analysis lays the fundamental groundwork for future searches for HNLs in IceCube.

Todo list

Write introduction (RED)	1
highlight a few more neutrino related open questions, to circle back to related to the HNL searches maybe? (YELLOW)	8
add Majorana condition and mention what this means for interactions (LNV of 2) (ORANGE)	9
Discuss lepton number conservation (pure dirac) and lepton number violation (dirac+majorana) (ORANGE)	9
elaborate on Leptogenesis in ν MSM and sterile neutrino DM, or link some papers? (ORANGE)	10
I think here I'd want the extended leptonic EW lagrangien, so I can explain the mass mixing and the interactions it opens up (RED)	10
mention KENU, Belle, L3 in the text and add references (RED)	11
mention PSI, LSND, NA3 in the text and add references (RED)	12
mention the Z boson decay results from DELPHI (because they are strong in Utau4, too (RED))	12
Say something about atmospheric neutrino flux uncertainties, based on recent JP/Anatoli papers. (YELLOW)	16
say something about matter effect? (ORANGE)	17
say something about mass ordering? (ORANGE)	17
Adapt chapter to reflect switched chapter order (RED)	23
put a number on this significant increase? (YELLOW)	25
put a number on the tilt angle? (YELLOW)	26
Include some low level plots like the trigger efficiency for the HNL simulation (ORANGE)	28
add example plots (2?) for L3 cut variables and applied cuts (YELLOW)	29
add some figure showing the corridors? (YELLOW)	30
add table with rates per level (split in flavor) - maybe better in analysis chapter to also show signal? (RED)	31
add image with selected strings used for flercnn IC and DC (YELLOW)	31
add some performance plots of the FLERCNN reconstruction (ORANGE)	32
There is more information on pre-processing the samples and preparing the input features, and training each cnn, but I'm not sure if that might be too much detail? (YELLOW)	32
add reference for flercnn analysis internal note (ORANGE)	32
which experiments measure the axial mass? (ORANGE)	35
cite this? (YELLOW)	37

Contents

Foreword	iii
Abstract	v
Contents	ix
1 Introduction	1
2 Standard Model Neutrinos and Beyond	5
2.1 The Standard Model	5
2.1.1 Fundamental Fields	5
2.1.2 Electroweak Symmetry Breaking	6
2.1.3 Fermion Masses	7
2.1.4 Leptonic Weak Interactions after Symmetry Breaking	7
2.2 Beyond the Standard Model	7
2.2.1 Mass Mechanisms	8
2.2.2 Minimal Extensions and the ν MSM	9
2.2.3 Observational Avenues for Right-Handed Neutrinos	10
2.3 Atmospheric Neutrinos as Source of Heavy Neutral Leptons	15
2.3.1 Production of Neutrinos in the Atmosphere	15
2.3.2 Neutrino Oscillations	16
2.3.3 Neutrino Interactions with Nuclei	18
2.3.4 Heavy Neutral Lepton Production and Decay	19
3 Standard Model Background Simulation and Data Processing	23
3.1 Event Generation	23
3.1.1 Neutrinos	24
3.1.2 Muons	25
3.2 Detector Simulation	25
3.2.1 Photon Propagation	25
3.2.2 Detector Responses	26
3.3 Processing	27
3.3.1 Trigger and Filter	28
3.3.2 Event Selection	29
3.4 Reconstruction	31
3.4.1 Fast Low Energy Reconstruction using Convolutional Neural Networks	31
3.4.2 Analysis Selection	32
3.5 Systematic Uncertainties	33
3.5.1 Atmospheric Flux Uncertainties	34
3.5.2 Cross-Section Uncertainties	35
3.5.3 Detector Calibration Uncertainties	36
3.5.4 Muon Uncertainties	37
Figures	39
Tables	41
Bibliography	43

Write introduction (RED)

The observation of neutrino oscillations has established that neutrinos have non-zero masses. This phenomenon is not explained by the standard model of particle physics, but one viable explanation to this dilemma is the existence of *heavy neutral leptons (HNLs)*, in the form of right-handed neutrinos with masses much larger than the observed neutrino masses ($\gg \text{eV}$). Depending on their mass and coupling to standard model neutrinos, these particles could also play an important role in solving further problems such as baryogenesis or serve as dark matter candidates.

This work presents the first search for HNLs with the IceCube Neutrino Observatory. The standard three flavor neutrino model is extended by adding a fourth GeV-scale mass state and allowing mixing with the tau neutrino through the mixing parameter $|U_{\tau 4}|^2$. The strength of this mixing is tested using atmospheric neutrinos as a source flux. Muon neutrinos that oscillated into tau neutrinos can produce HNLs through neutral current interactions, which then decay back to standard model particles. Both production and decay may produce observable light in the detector, leading to a unique signature of two cascades at low energies.

The measurement is performed through a binned, maximum likelihood fit, comparing the observed data to the expected events from atmospheric neutrinos and HNLs. Three HNL mass values, m_4 , of 0.3 GeV, 0.6 GeV, and 1.0 GeV are tested using ten years of data, collected between 2011 and 2021. The fits constrain the mixing parameter to $|U_{\tau 4}|^2 < 0.19$ ($m_4 = 0.3 \text{ GeV}$), $|U_{\tau 4}|^2 < 0.36$ ($m_4 = 0.6 \text{ GeV}$), and $|U_{\tau 4}|^2 < 0.40$ ($m_4 = 1.0 \text{ GeV}$) at 90% confidence level. No significant signal of HNLs is observed for any of the tested masses, and the best fit mixing values obtained are consistent with the null hypothesis of no mixing.

Additionally, a thorough investigation of the unique low energy double cascade signature of HNLs in IceCube is performed. A benchmark reconstruction performance is estimated using a well established IceCube reconstruction tool, after optimizing it for low energy double cascade events. The limitations of the detector to observe these events are identified, and their origins are discussed. This first analysis lays the fundamental groundwork for future searches for HNLs in IceCube.

notes for the introduction

- ▶ observation of non-zero neutrino masses indicates likely existence of new physics beyond the standard model
- ▶ multiple SM neutral fermions (right handed) could explain the neutrino masses and their smallness
- ▶ if they are heavy enough to not be produced in oscillations, they are called heavy neutral leptons
- ▶
- ▶ In 1984 the PS191 [G. Bernardi et al., Phys. Lett. B 166, 479 (1986), G. Bernardi et al., Phys. Lett. B 203, 332 (1988)] experiment at CERN

appears to have been the earliest beam dump to report HNL bounds from the direct production and decay.



During my time at desy and in IceCube, I have been involved in several projects, which are not all directly related to the main analysis presented in this thesis. I will give a brief overview of my scientific contributions and how they are related to the main analysis.

In close collaboration with a former colleague (Alex Trettin), we developed a novel method to treat detector uncertainty effects in IceCube, which we documented in a few author paper, and which is now one of the default method to incorporate detector uncertainties in atmospheric neutrino analyses in IceCube. This method will also be used in the main analysis of this thesis and is briefly introduced in Section ??.

Throughout the last years, I was also involved in updating and maintaining the open source analysis framework PISA, which is used in many analyses.

Work related (what is my original work):

- the model independent simulation chain described in Section ?? was developed exclusively by myself
- for the model dependent generator presented in Section ??, the skeletal structure was constructed by collaborators, before I took over and implemented the full model dependent simulation chain, including the correct decay widths calculations, custom cross-section, and the weighting scheme, continuously optimizing and testing it, before producing and processing the full samples for the main analysis
- both the study on how well IceCube can detect low energy double cascades in Chapter ?? and the main analysis in Chapter ?? were developed and performed by myself independently and are original work

[1]: Pauli (1978), "Dear radioactive ladies and gentlemen"

[2]: Cowan et al. (1956), "Detection of the Free Neutrino: a Confirmation"

[3]: Danby et al. (1962), "Observation of High-Energy Neutrino Reactions and the Existence of Two Kinds of Neutrinos"

[4]: Kodama et al. (2001), "Observation of tau neutrino interactions"

[5]: Davis et al. (1968), "Search for Neutrinos from the Sun"

The neutrino was postulated by Wolfgang Pauli [1] in 1930 to explain the continuous energy spectrum of electrons originating from beta decay. Cowan and Reines confirmed this prediction of a light, neutral particle in 1956 when they discovered the electron neutrino using inverse beta decay [2]. Two additional neutrino flavors were found in the following years, and with the discovery of the muon neutrino in 1962 [3] and the tau neutrino in 2001 [4], the current theory of neutrinos in the standard model (SM) was established.

Although neutrinos were first believed to be massless, experimental evidence showing the existence of mixed neutrino states started to appear in the 1960s [5]. Mixing between different physical representations of neutrinos is proof for differences in their masses. The resulting phenomenon of neutrino oscillations can be incorporated into the standard model by extending it to include massive neutrinos. How massive they are and how strong is the mixing between neutrino states has to be obtained from measurement. Today there are a variety of precision oscillation experiments using solar, reactor and atmospheric neutrinos to tighten the constraints on the neutrino oscillation parameters. IceCube is one of those leading experiments probing the oscillation theory with atmospheric neutrinos.

[6]: Aartsen et al. (2017), "The IceCube Neutrino Observatory: instrumentation and online systems"

The IceCube Neutrino Observatory [6] was constructed between 2004 and 2010 at the geographic South Pole. It is the first cubic kilometer Cherenkov

neutrino detector and consists of 5160 optical sensors attached to 86 strings, drilled down to a maximum depth of ~ 2500 m into the Antarctic ice. Neutrinos are detected by the Cherenkov light that is emitted by secondary particles produced in neutrino-nucleon scattering interactions in the ice. With DeepCore, a more densely instrumented sub-array of IceCube, the neutrino detection energy threshold can be lowered to approximately 5 GeV.

At these energies, the similarity in event signatures poses difficulties in identifying different neutrino flavor interactions. Muon neutrino charged-current interactions produce light tracks as opposed to charged-current interactions of electron and tau neutrinos as well as neutral-current interactions of all neutrinos that produce light cascades. The sparse instrumentation of IceCube makes it more challenging to separate track- and cascade-like events. In this thesis, a novel method to distinguish those two event types is developed. In contrast to previously used univariate separation techniques, the multivariate machine learning method applied here maximizes the use of information from the detector response. Through the use of a Gradient Tree Boosting algorithm the separation of events in track and cascade is improved. As a result of the improved separation, the uncertainty to the atmospheric neutrino oscillation parameters Δm_{32}^2 and θ_{23} is significantly reduced.

Standard Model Neutrinos and Beyond

2

2.1 The Standard Model

The SM of particle physics is a Yang-Mills theory [7] providing very accurate predictions of weak, strong, and *electromagnetic* (EM) interactions. It is a relativistic quantum field theory that relies on gauge invariance, where all matter is made up of fermions, which are divided into quarks and leptons, and bosons describe the interactions between the fermions that have to fulfil the overall symmetry of the theory. Leptons are excitations of Dirac-type fermion fields.

The initial idea of the theory is associated with the works of Weinberg [8], Glashow [9], and Salam [10], that proposed a unified description of EM and weak interactions as a theory of a spontaneously broken $SU(2) \times U(1)$ symmetry for leptons, predicting a neutral massive vector boson Z^0 , a massive charged vector boson W^\pm , and a massless photon γ as the gauge bosons. The Higgs mechanism [11], describing the breaking of the symmetry, predicts the existence of an additional scalar particle, the Higgs boson, giving the W^\pm and Z^0 bosons their mass. The Higgs boson was discovered in 2012 at the LHC [12, 13].

Gell-Mann and Zweig proposed the quark model in 1964 [14, 15], which was completed by the discovery of non-abelian gauge theories [16] to form the $SU(3)$ symmetry of the strong interaction called *quantum chromodynamics* (QCD). QCD describes the interaction between quarks and gluons which completed the full picture of the SM in the mid-1970s. Together with the electroweak theory, the SM is a $SU(3)_C \times SU(2)_L \times U(1)_Y$ local gauge symmetry, with the conserved quantities C , *color*, L , *left-handed chirality*, and Y , *weak hypercharge*.

In the following, the basic properties of the SM are described, following the derivations of [17, 18].

2.1.1 Fundamental Fields

Fermions in the SM are Weyl fields with either *left-handed* (LH) or *right-handed* (RH) chirality, meaning they are eigenvectors of the chirality operator γ_5 with $\gamma_5 \psi_{R/L} = \pm \psi_{R/L}$. Only LH particles transform under $SU(2)_L$. The Higgs field is a complex scalar field, a doublet of $SU(2)_L$, which is responsible for the spontaneous symmetry breaking of $SU(2)_L \times U(1)_Y$ to $U(1)_{EM}$. Local gauge transformations of the fields are given by

$$\psi \rightarrow e^{ig\theta^a(x)T^a} \psi, \quad (2.1)$$

where g is the coupling constant, $\theta^a(x)$ are the parameters of the transformation, and T^a are the generators of the group, with a counting them. The number of bosons is dependent on the generators of the symmetry groups, while the strength is defined by the coupling constants. There are eight massless gluons corresponding to the generators of the $SU(3)_C$ group. These

2.1	The Standard Model	5
2.2	Beyond the Standard Model	7
2.3	Atmospheric Neutrinos as Source of Heavy Neutral Leptons . . .	15

[7]: Yang et al. (1954), “Conservation of Isotopic Spin and Isotopic Gauge Invariance”

[8]: Weinberg (1967), “A Model of Leptons”

[9]: Glashow (1961), “Partial-symmetries of weak interactions”

[11]: Higgs (1964), “Broken symmetries, massless particles and gauge fields”

[12]: Chatrchyan et al. (2012), “Observation of a New Boson at a Mass of 125 GeV with the CMS Experiment at the LHC”

[13]: Aad et al. (2012), “Observation of a new particle in the search for the Standard Model Higgs boson with the ATLAS detector at the LHC”

[14]: Gell-Mann (1964), “A Schematic Model of Baryons and Mesons”

[15]: Zweig (1964), “An $SU(3)$ model for strong interaction symmetry and its breaking. Version 2”

[17]: Giunti et al. (2007), *Fundamentals of Neutrino Physics and Astrophysics*

[18]: Schwartz (2013), *Quantum Field Theory and the Standard Model*

mediate the strong force which conserves color charge. The W_1, W_2, W_3 , and B boson fields of the $SU(2)_L \times U(1)_Y$ group are mixed into the massive bosons through spontaneous symmetry breaking as

$$W^\pm = \frac{1}{\sqrt{2}}(W_1 \mp iW_2) \quad (2.2)$$

and

$$Z^0 = \cos \theta_W W_3 - \sin \theta_W B, \quad (2.3)$$

with θ_W being the *Weinberg angle*. The massless photon field is given by

$$A = \sin \theta_W W_3 + \cos \theta_W B \quad (2.4)$$

and its conserved quantity is the EM charge Q , which depends on the weak hypercharge, Y , and the third component of the weak isospin, T_3 , as $Q = T_3 + Y/2$.

	Type			Q
quarks	u	c	t	+2/3
	d	s	b	-1/3
leptons	ν_e	ν_μ	ν_τ	0
	e	μ	τ	-1

Table 2.1: Fermions in the Standard Model. Shown are all three generations of quarks and leptons with their electric charge Q .

Fermions are divided into six quarks and six leptons. Weak, strong, and EM force act on the quarks, and they are always found in bound form as baryons or mesons. Leptons do not participate in the strong interaction and only the electrically charged leptons are massive and are effected by the EM force, while neutrinos are massless and only interact via the weak force. Each charged lepton has an associated neutrino, which it interacts with in *charged-current* (CC) weak interactions, that will be explained in more detail in Section 2.1.4. The fermions are listed in Table 2.1.

2.1.2 Electroweak Symmetry Breaking

To elaborate the process of spontaneous symmetry breaking through which the gauge bosons of the weak interaction acquire their masses, the Lagrangian of the Higgs field is considered as

$$\mathcal{L}_{\text{Higgs}} = (D_\mu \Phi^\dagger)(D^\mu \Phi) - \lambda \left(\Phi^\dagger \Phi - \frac{v^2}{2} \right)^2, \quad (2.5)$$

with parameters λ and v , where λ is assumed to be positive. Φ is the Higgs doublet, which is defined as

$$\Phi = \begin{pmatrix} \Phi^+ \\ \Phi^0 \end{pmatrix}, \quad (2.6)$$

with the charged component Φ^+ and the neutral component Φ^0 . The covariant derivative is given by

$$D_\mu = \partial_\mu - ig_2 \frac{\sigma^i}{2} W_\mu^i - \frac{1}{2} ig_1 B_\mu, \quad (2.7)$$

with the Pauli matrices σ^i and the gauge boson fields W_μ^i and B_μ of the $SU(2)_L$ and $U(1)_Y$ groups, respectively. The coupling constants g_2 and g_1 are the respective coupling constants which are related to the Weinberg angle as $\tan \theta_W = \frac{g_1}{g_2}$. The Higgs potential has a non-zero *vacuum expectation value* (v) at the minimum of the potential at $\Phi^\dagger \Phi = \frac{v^2}{2}$. Since the vacuum is electrically neutral, it can only come from a neutral component of the Higgs

doublet as

$$\Phi_{\text{vev}} = \frac{1}{\sqrt{2}} \begin{pmatrix} 0 \\ v \end{pmatrix}. \quad (2.8)$$

2.1.3 Fermion Masses

The mass term for charged fermions with spin-1/2 is given by

$$\mathcal{L}_{\text{Dirac}} = m(\bar{\Psi}_R \Psi_L - \bar{\Psi}_L \Psi_R), \quad (2.9)$$

composed of the product of LH and RH Weyl spinors $\Psi_{L/R}$. This term is not invariant under $SU(2)_L \times U(1)_Y$ gauge transformations, but adding a Yukawa term

$$\mathcal{L}_{\text{Yukawa}} = -Y^e \bar{L}_L \Phi e_R + h.c., \quad (2.10)$$

coupling the fermion fields e_R to the Higgs field Φ , recovers the invariance and gives the fermions their masses. Here, Y^e is the Yukawa coupling constant and \bar{L}_L is the $SU(2)_L$ doublet. With the vev, this results in the mass term for the charged leptons and down-type quarks of $-m_e(\bar{e}_L e_R + \bar{e}_R e_L)$ with $m_e = \frac{Y^e v}{\sqrt{2}}$. With $\tilde{\Phi} = i\sigma_2 \Phi^*$, a similar Yukawa term can be written as $-Y^u \bar{L}_L \tilde{\Phi} u_R + h.c.$, which leads to the masses of the up-type quarks.

2.1.4 Leptonic Weak Interactions after Symmetry Breaking

After the spontaneous symmetry breaking, the leptonic part of the electroweak Lagrangian can be written as

$$\begin{aligned} \mathcal{L}_{\text{EW}}^\ell = & \frac{g}{\sqrt{2}} W^+ \sum_{\alpha=e,\mu,\tau} \bar{\nu}_\alpha \gamma^\mu P_L \ell_\alpha + \frac{g}{4c_w} Z \\ & \times \left\{ \sum_{\alpha=e,\mu,\tau} \bar{\nu}_\alpha \gamma^\mu P_L \nu_\alpha + \sum_\alpha \bar{\ell}_\alpha \gamma^\mu [2s_w^2 P_R - (1 - 2s_w^2) P_L] \ell_\alpha \right\} + h.c., \end{aligned} \quad (2.11)$$

where $c_w \equiv \cos \theta_w$, $s_w \equiv \sin \theta_w$, P_L and P_R are the left and right projectors, respectively, while ν_α and ℓ_α are the neutrino and charged lepton weak eigenstates. The W^\pm and Z bosons are the massive gauge bosons of the weak interaction. The large boson masses $m_W \sim 80 \text{ GeV}$ and $m_Z \sim 90 \text{ GeV}$ result in a short range of the force of about $1 \times 10^{-18} \text{ m}$. Interactions carried out by the W^\pm bosons are called *charged current (CC)* interactions, as they propagate a charge, therefore changing the interacting lepton to its charged/neutral counterpart. *Neutral current (NC)* interactions are those mediated by the Z^0 boson, where no charge is transferred. NC interactions couple neutrinos to neutrinos and charged leptons to charged leptons, but not to each other. The Feynman diagrams for CC and NC interactions are shown in Figure 2.1.

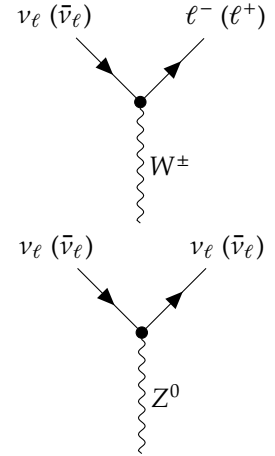


Figure 2.1: Feynman diagrams of charged-current (top) and neutral-current (bottom) neutrino weak interactions, modified from [19].

2.2 Beyond the Standard Model

The fundamentals of the SM described above **are not** enough to explain all observed phenomena. Gravity cannot be explained by the SM, as it is incompatible with general relativity, neither can some of the cosmological observations like DM, and the matter-antimatter asymmetry be explained. But most importantly, the SM does not predict neutrinos to have mass, which

[20]: Deruelle et al. (2018), *Relativity in Modern Physics*

[21]: Workman et al. (2022), "Review of Particle Physics"

[22]: Fukugita et al. (1986), "Baryogenesis without grand unification"

[5]: Davis et al. (1968), "Search for Neutrinos from the Sun"

[23]: Fukuda et al. (1998), "Evidence for Oscillation of Atmospheric Neutrinos"

[24]: Ahmad et al. (2002), "Direct Evidence for Neutrino Flavor Transformation from Neutral-Current Interactions in the Sudbury Neutrino Observatory"

[25]: Alam et al. (2021), "Completed SDSS-IV extended Baryon Oscillation Spectroscopic Survey: Cosmological implications from two decades of spectroscopic surveys at the Apache Point Observatory"

[26]: Aghanim et al. (2020), "Planck2018 results: VI. Cosmological parameters"

[27]: Aker et al. (2022), "Direct neutrino-mass measurement with sub-electronvolt sensitivity"

highlight a few more neutrino related open questions, to circle back to related to the HNL searches maybe? (YELLOW)

is experimentally proven by neutrino oscillations, so some extension to the SM is needed in order to explain the observed phenomena.

The standard cosmological model Λ CDM [20] assumes that equal amounts of matter and anti-matter were produced in the early universe. However, the universe today is dominantly made up of matter. This BAU can be measured by the difference between the number densities of baryons and anti-baryons normalized to the number density of photons as

$$\eta_B = \frac{n_B - n_{\bar{B}}}{n_\gamma}, \quad (2.12)$$

where n_B , $n_{\bar{B}}$, and n_γ are the number densities of baryons, anti-baryons, and photons, respectively. Baryons are the dominant component with η_B being observed to be at the order of 10^{-9} [21]. Leptogenesis and EW baryogenesis are scenarios that could explain this phenomenon, where the former could be realized by the existence of heavy RH neutrinos [22].

The observation of neutrino flavor conversions and neutrino oscillations in a multitude of experiments [5, 23, 24] is the strongest evidence for physics *beyond the standard model* (BSM) measured in laboratories to date. The observation that neutrinos change their flavor while they propagate through space can only be explained, if at least two neutrinos have a non-zero mass. From those measurements we know the mass differences are very small as compared to the lepton masses, but neither their existence, nor their smallness is predicted by the SM. There are upper limits on the sum of all neutrino masses from cosmological observations at 1.2 eV [25, 26] and at 0.8 eV from the KATRIN experiment [27]. Adding RH neutrino states to the theory could explain the origin of the observed non-zero neutrino masses and could be tested for by searching for corresponding signatures in experiments.

2.2.1 Mass Mechanisms

Since there are no RH neutrinos in the SM, the mass mechanism described in Section 2.1.3, which couples the Higgs field to LH and RH Weyl fields, predicts the LH neutrinos to be massless. From experimental observations it is known that at least two of the three neutrino generations need to have a non-zero mass. Assuming the existence of RH neutrinos fields ν_R , one way of producing the neutrino masses is by adding a Yukawa coupling term similar to the one for up-type quarks mentioned in Section 2.1.3, to write the full Yukawa Lagrangian as

$$\mathcal{L}_{\text{Yukawa}} = -Y_{ij}^e \bar{L}_L^i \Phi e_R^j - Y_{ij}^\nu \bar{L}_L^i \tilde{\Phi} \nu_R^j + h.c., \quad (2.13)$$

with i, j running over the three generations of leptons e, μ , and τ , and Y^e and Y^ν being the Yukawa coupling matrices. Diagonalizing the Yukawa coupling matrices through unitary transformations U^e and U^ν leads to the **Dirac mass term** in the mass basis as

$$\mathcal{L}_{\text{Dirac}}^{\text{mass}} = \frac{v}{\sqrt{2}} (\bar{e}_L M_e e_R - \bar{\nu}_L M_\nu \nu_R), \quad (2.14)$$

where M_e and M_ν are the diagonal mass matrices of leptons and neutrinos, respectively. A purely Dirac mass term would not explain the smallness of

the neutrino masses in a straightforward way. Only fine-tuning the Yukawa coupling constants to small values would lead to small neutrino masses.

An additional way of generating neutrino masses is by adding a Majorana mass term of the form

$$\mathcal{L}_{\text{Majorana}} = -\frac{1}{2}M_{ij}(\nu_R^i)^c \nu_R^j + h.c. , \quad (2.15)$$

with M_{ij} being the Majorana mass matrix and the indices i, j running over all n_R RH neutrino generations. The superscript c denotes the charge conjugate field. Combining the charge conjugated RH neutrino fields with the LH neutrino fields as

$$N = \begin{pmatrix} \nu_L \\ \nu_R^c \end{pmatrix} , \quad (2.16)$$

with ν_R containing the n_R RH fields. The full neutrino mass Lagrangian is then given by the combined **Dirac and Majorana mass term** as

$$\mathcal{L}_{\text{Dirac+Majorana}}^{\text{mass},\nu} = \frac{1}{2}N^T \hat{C} M^{\text{D+M}} N + h.c. , \quad (2.17)$$

and the mass matrix is given by

$$M^{\text{D+M}} = \begin{pmatrix} 0 & (M^{\text{D}})^T \\ M^{\text{D}} & M^{\text{R}} \end{pmatrix} . \quad (2.18)$$

On top of explaining the origin of neutrino masses itself, a combined Dirac and Majorana mass term could also solve the question of their smallness. If the mass of the RH neutrinos is very large, the masses of the active neutrino flavors is suppressed, which is known as *see-saw mechanism*.

2.2.2 Minimal Extensions and the ν MSM

So far we have described neutrinos in their flavor eigenstates, which are relevant for weak interactions, where the three weak flavor states ν_e, ν_μ , and ν_τ are related to the charged leptons they interact with in CC interactions. In order to *just* explain the three oscillating flavor eigenstates, three mass states are needed, which are related to the flavor eigenstates by the unitary, 3×3 Pontecorvo-Maki-Nakagawa-Sakata (PMNS) mixing matrix U , where the flavor states are a superposition of the mass states as

$$|\nu_\alpha\rangle = \sum_k U_{\alpha k}^* |\nu_k\rangle , \quad (2.19)$$

with the weak flavor states $|\nu_\alpha\rangle$, $\alpha = e, \mu, \tau$, and the mass states $|\nu_k\rangle$ with $k = 1, 2, 3$. In its generic form the PMNS matrix is given by

$$U = \begin{pmatrix} U_{e1} & U_{e2} & U_{e3} \\ U_{\mu1} & U_{\mu2} & U_{\mu3} \\ U_{\tau1} & U_{\tau2} & U_{\tau3} \end{pmatrix} , \quad (2.20)$$

which will be the basis for the discussion of neutrino oscillations in Section 2.3.2.

This however is not enough to explain the neutrino masses observed in oscillation experiments. The most minimal model required to give rise to two non-zero active neutrino masses, is an additional two RH neutrinos,

add Majorana condition and mention what this means for interactions (LNV of 2) (ORANGE)

Discuss lepton number conservation (pure dirac) and lepton number violation (dirac+majorana) (ORANGE)

[28]: Asaka et al. (2005), “The nuMSM, dark matter and neutrino masses”

[29]: Asaka et al. (2005), “The ν MSM, dark matter and baryon asymmetry of the universe”

elaborate on Leptogenesis in ν MSM and sterile neutrino DM, or link some papers? (ORANGE)

[30]: Minkowski (1977), “ $\mu \rightarrow e \gamma$ at a rate of one out of 10^9 muon decays?”

[31]: Yanagida (1980), “Horizontal Symmetry and Masses of Neutrinos”

[32]: Glashow (1980), “The Future of Elementary Particle Physics”

[33]: Gell-Mann et al. (1979), “Complex Spinors and Unified Theories”

[34]: Mohapatra et al. (1980), “Neutrino Mass and Spontaneous Parity Nonconservation”

I think here I'd want the extended leptonic EW lagrangien, so I can explain the mass mixing and the interactions it opens up (RED)

[35]: Aartsen et al. (2020), “eV-Scale Sterile Neutrino Search Using Eight Years of Atmospheric Muon Neutrino Data from the IceCube Neutrino Observatory”

[19]: Trettin (2023), “Search for eV-scale sterile neutrinos with IceCube DeepCore”

[36]: Tastet et al. (2021), “Reinterpreting the ATLAS bounds on heavy neutral leptons in a realistic neutrino oscillation model”

assuming the mass of the lightest SM neutrino is zero. If the additional neutrino states have masses $\gg eV$ they are referred to as HNL, which are almost sterile, with a small mass mixing with the active neutrinos.

But the SM also fails to explain additional observations of physics beyond the standard model (BAU, DM), which could be solved by the *neutrino minimal standard model* (ν MSM) [28, 29]. In the ν MSM, three RH neutrinos are added, where two of them are heavy, to explain the observed neutrino masses and oscillations, and a third one is light and serves as a DM candidate. The mixing between mass and flavor eigenstates is then described by an extended 6x6 mixing matrix as

$$\begin{pmatrix} \nu_e \\ \nu_\mu \\ \nu_\tau \\ N_1 \\ N_2 \\ N_3 \end{pmatrix} = \begin{pmatrix} U_{e1} & U_{e2} & U_{e3} & U_{e4} & U_{e5} & U_{e6} \\ U_{\mu1} & U_{\mu2} & U_{\mu3} & U_{\mu4} & U_{\mu5} & U_{\mu6} \\ U_{\tau1} & U_{\tau2} & U_{\tau3} & U_{\tau4} & U_{\tau5} & U_{\tau6} \\ U_{N_11} & U_{N_12} & U_{N_13} & U_{N_14} & U_{N_15} & U_{N_16} \\ U_{N_21} & U_{N_22} & U_{N_23} & U_{N_24} & U_{N_25} & U_{N_26} \\ U_{N_31} & U_{N_32} & U_{N_33} & U_{N_34} & U_{N_35} & U_{N_36} \end{pmatrix} \begin{pmatrix} \nu_1 \\ \nu_2 \\ \nu_3 \\ \nu_4 \\ \nu_5 \\ \nu_6 \end{pmatrix}, \quad (2.21)$$

where N_i and ν_{i+3} ($i \in [1, 2, 3]$) are the sterile flavor states and the additional RH mass states, respectively. In the ν MSM, the two heavy RH neutrinos generate the active neutrino masses through the type I seesaw mechanism [30–34], where they are assumed to be SM scalars and couple to the Higgs field as such.

2.2.3 Observational Avenues for Right-Handed Neutrinos

If the RH neutrinos have masses at the eV scale, they can be observed through distortion effects in measurements of neutrino oscillation experiments. Several analyses looking for these so-called light sterile neutrinos exist in IceCube, where [35] is using atmospheric neutrinos in the higher energy range of 500 GeV to 10 000 GeV and [19] is using the lower energy region of 6 GeV to 156 GeV. The latter work includes a detailed description of the expected oscillation effects and the various anomalies observed in oscillation experiments that could be explained by the existence of a light sterile neutrino, which is not covered in this work.

Here, the focus will be on heavy RH neutrinos, interchangeably also called heavy sterile neutrinos, or HNLs. A defining property is that they are too massive to be produce in oscillations and to be observed as distortions thereof. Several ways to observe HNLs are possible through direct production and decay experiments, which will be discussed in the following. Most of the existing searches assume the minimal model, where only one coupling between the new mass states and the SM neutrinos is non-zero and the coupling is just through mass mixing in a type I seesaw scenario, but more complex scenarios are of course also possible and might produce various additional signatures, or stronger signals.

In general, the constraints discussed in the following are based on models, where only the coupling between the HNL and one SM flavor is non-zero. While this is the straight forward approach to test the mixing parameters individually, this might make the constraints stronger than they would be in a more complex scenario, where the HNLs couple to more than one SM flavor as was show in [36] for collider bounds.

Extracted Beamline Searches

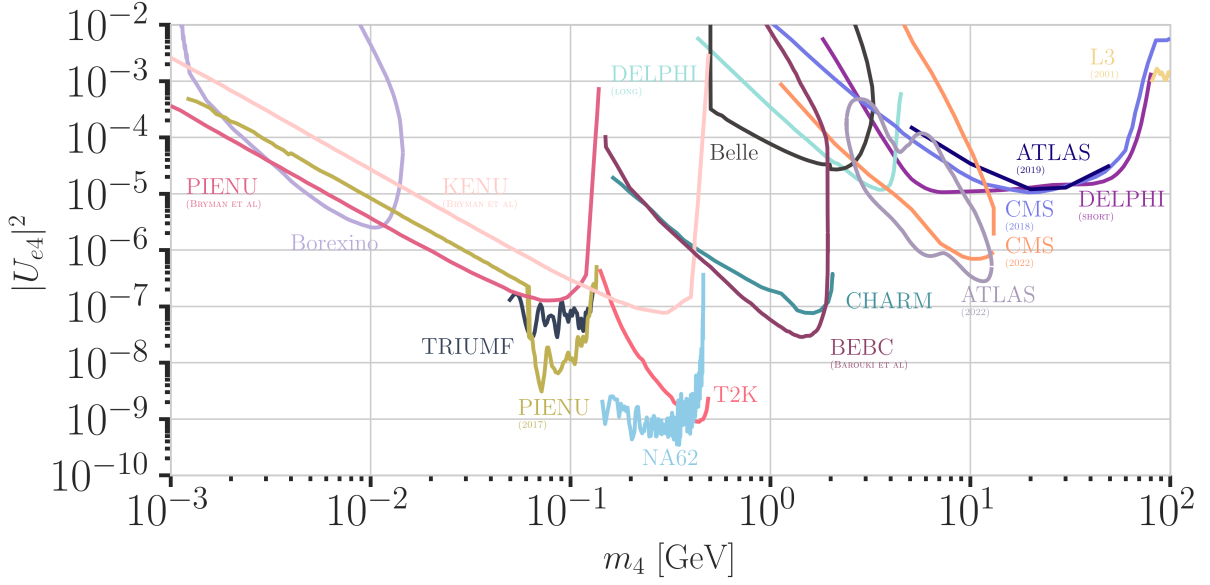


Figure 2.2: Current leading $|U_{e4}|^2 - m_4$ limits from PIENU [37, 38], BOREXINO [39], KENU [43], BEBC [44], Belle, L3, CHARM [45], ATLAS [46, 47], CMS [48, 49], and NuTeV [50]. Modified from [43] in the text and add references (RED)

Protons interacting with a target or a beam dump can produce Pions, Kaons, and heavy-quark hadrons, whose subsequent decays would also produce HNLs. The energies of the HNLs produced in those interactions are between 1 MeV and 4 GeV and could decay at several distances, depending on their lifetime, which is model dependent. Experiments along the extracted beamline, which are using a spectrometer with particle identification, can search for unique decay signatures at displaced vertices. Example signatures are $\nu_4 \rightarrow l_\alpha \pi$, $\nu_4 \rightarrow l_\alpha^+ l_\alpha^-$, or $\nu_4 \rightarrow \nu \pi^0$ (or other neutral mesons), which cannot be explained by SM neutrinos. Depending on the decay channel, a specific mixing can be probed. The other way of searching for HNLs with these interactions is to look for peaks in the missing mass spectrum, measured around the production vertex at the target, which usually is not possible for beam dumps, as the beam dump region is not calorimetrically instrumented.

HNL search pioneer work was done by experiments at extracted beam lines, with first results from *PS191* [52] and *CHARM* [45], reporting bounds from direct production and decay of HNLs for $|U_{e4}|^2$, $|U_{\mu 4}|^2$, and combinations of them, at masses from 10 MeV to 500 MeV at orders of 10^{-3} to 10^{-6} . Since then, there has been and still is a large activity of searches for HNLs at extracted beamlines and the strongest bounds on $|U_{e4}|^2$ and $|U_{\mu 4}|^2$ are currently set by *PIENU* [37, 38, 53], *TRIUMF* [40], *NA62* [41], *T2K* [42], *BNL-E949* [54], *MicroBooNE* [55], and *NuTeV* [50] in the mass range from 1 MeV to 4 GeV, reaching from 10^{-4} at the lower mass to 10^{-9} at 4 at the highest masses. The current strongest bounds are shown in Figure 2.2 and Figure 2.3, which also shows bounds from other experiments, which will be discussed in the following.

Especially noteworthy are the results of analyses probing the mixing with the third lepton generation, $|U_{\tau 4}|^2$, from *NOMAD* [56] and reinterpretations of the *CHARM* results and the *BEBC* results in the context of the mixing

- [52]: Bernardi et al. (1986), “Search for Neutrino Decay”
- [45]: Bergsma et al. (1983), “A Search for Decays of Heavy Neutrinos”
- [37]: Bryman et al. (2019), “Constraints on Sterile Neutrinos in the MeV to GeV Mass Range”
- [38]: Aguilar-Arevalo et al. (2018), “Improved search for heavy neutrinos in the decay $\pi \rightarrow e \nu$ ”
- [53]: Ito et al. (2021), “Search for heavy neutrinos in $\pi^+ \rightarrow \mu^+ \nu$ decay and status of lepton universality test in the PIENU experiment”
- [40]: Britton et al. (1992), “Improved search for massive neutrinos in $\pi^+ \rightarrow e^+ \nu$ decay”
- [41]: Parkinson et al. (2022), “Search for heavy neutral lepton production at the NA62 experiment”
- [42]: Abe et al. (2019), “Search for heavy neutrinos with the T2K near detector ND280”
- [54]: Artamonov et al. (2015), “Search for heavy neutrinos in $K^+ \rightarrow \mu^+ \nu_H$ decays”
- [55]: Abratenko et al. (2024), “Search for Heavy Neutral Leptons in Electron-Positron and Neutral-Pion Final States with the MicroBooNE Detector”
- [50]: Vaitaitis et al. (1999), “Search for neutral heavy leptons in a high-energy neutrino beam”
- [56]: Astier et al. (2001), “Search for heavy neutrinos mixing with tau neutrinos”

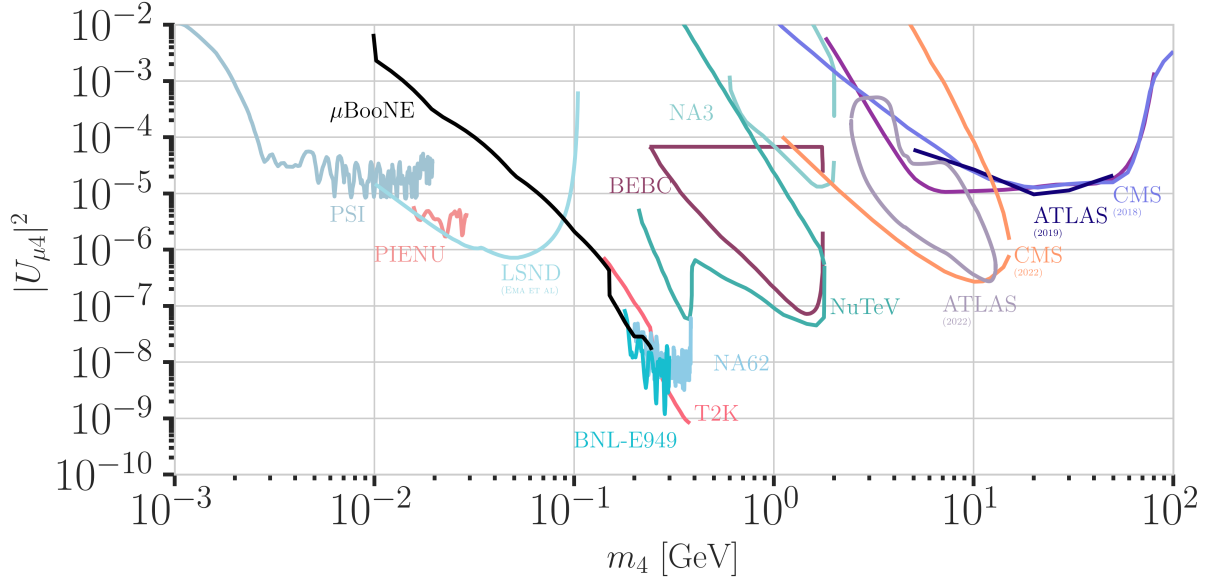


Figure 2.3: Current leading $|U_{\mu 4}^2| - m_4$ limits from PSI , μ BooNE [55], PIENU [37], LSND , BNL-E949 [54], NA62 [41], T2K [42], BEBC [59], ATLAS [46, 47], CMS [48, 49], NuTeV [50], and NA3 . Modified from [51]. Modified from [51].

[44]: Barouki et al. (2022), “Blast from the past II: Constraints on heavy neutral leptons from the BEBC WA66 beam dump experiment”

[57]: Orloff et al. (2002), “Limits on the mixing of tau neutrino to heavy neutrinos”

[58]: Boiarska et al. (2021), “Blast from the past: constraints from the CHARM experiment on Heavy Neutral Leptons with tau mixing”

mention PSI, LSND, NA3 in the text and add references (RED)

[46]: Aad et al. (2019), “Search for heavy neutral leptons in decays of W bosons produced in 13 TeV pp collisions using prompt and displaced signatures with the ATLAS detector”

[47]: Aad et al. (2023), “Search for Heavy Neutral Leptons in Decays of W Bosons Using a Dilepton Displaced Vertex in $\sqrt{s} = 13\text{TeV}$ pp Collisions with the ATLAS Detector”

[48]: Sirunyan et al. (2018), “Search for heavy neutral leptons in events with three charged leptons in proton-proton collisions at $\sqrt{s} = 13\text{ TeV}$ ”

[49]: Tumasyan et al. (2022), “Search for long-lived heavy neutral leptons with displaced vertices in proton-proton collisions at $\sqrt{s} = 13\text{ TeV}$ ”

[60]: Shuve et al. (2016), “Revision of the LHCb Limit on Majorana Neutrinos”

[61]: Aaij et al. (2021), “Search for heavy neutral leptons in $W^+ \rightarrow \mu^+ \mu^\pm \text{jet}$ decays”

$|U_{\tau 4}|^2$, where the latter is place the most stringent limits from 10^{-3} to 10^{-6} in the 0.1 GeV to 2 GeV range [44, 57, 58]. In Figure 2.4 the current strongest bounds on $|U_{\tau 4}|^2$ are shown.

Collider Searches

So far, collider searches have been conducted at the *large electron positron collider (LEP)* and at the *large hadron collider (LHC)* in proton-proton mode. Strongest results are from the ATLAS and CMS experiments, which are nearly hermetic, general purpose detectors around the interaction point, and from the DELPHI and the LHCb experiments, which are forward detectors that can be used to search for new particles in decays of heavy particles produced. In the minimal model, HNLs in the GeV mass range can be produced through mass mixing in decays of heavy mesons, tau leptons, Z/W bosons, H bosons, or top quarks originating from the collisions. Depending on the dirac or majorana nature of the HNL, they can decay to lepton number conserving or lepton number violating channels.

Using prompt and displaced decays of the HNL, both ATLAS and CMS have set constraints on $|U_{e 4}|^2$ and $|U_{\mu 4}|^2$ at the level of 10^{-4} to 10^{-6} in the mass range between 1 GeV to 100 GeV [46–49]. The LHCb experiment has HNL search results at HNL masses below and above the W boson mass, where the low mass searches are using the decay channel $B^- \rightarrow \pi^+ \mu^- \mu^-$, setting limits at the 10^{-3} level for $|U_{\mu 4}|^2$ in the mass range of 0.5 GeV to 3.5 GeV [60]. At high masses, the $W^+ \rightarrow \mu^- \mu^\pm \text{jet}$ channel is used to set limits at the order of 10^{-3} to 10^{-2} for $|U_{\mu 4}|^2$ in the mass range of 5 GeV to 50 GeV in the LNC channel and at the order of 10^{-4} to 10^{-3} in the LNV channel [61].

Nuclear Decays Measurements

A novel approach of searching for irregularities in energy-momentum conservation measurements in nuclear reactions might be a viable way of

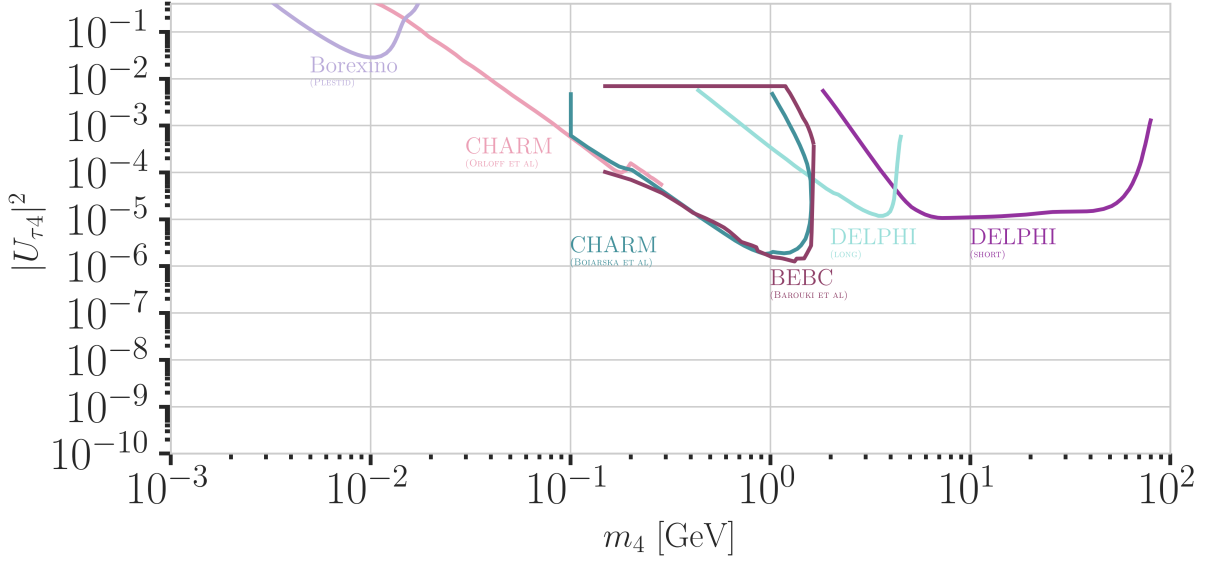


Figure 2.4: Current leading $|U_{\tau 4}|^2 - m_4$ limits from BOREXINO [62], CHARM [57, 58], DELPHI [43], and BEBC [44]. Modified from [51].

searching for HNLs, as they could be interpreted as constraints on $|U_{e4}|^2$ and m_4 .

Kinks in **beta decay** spectra would show up at $Q - m_4 c^2$, where the HNL mass, m_4 , can be measured between the lower energy detection threshold and the energy released in the decay, which is called Q value. Analyses using the tritium decay, with $Q = 18.6$ keV, are planned in *KATRIN* [63] and *TRISTAN* [64] in the 1 keV to 18 keV range. Their projected statistical limits are around 10^{-7} for $|U_{e4}|^2$, but will require further detector upgrades [64]. A first result from KATRIN measurements during commissioning sets limits at the order of 10^{-2} to 10^{-3} in the mass range of 0.1 keV to 1.6 keV [65]. *DUNE* is planning to measure the ionization charge of atmospheric argon decays, with $Q = 565$ keV, to probe $|U_{e4}|^2$ at in the 20 keV to 450 keV mass range. The projected sensitivity is at the 10^{-5} level, and might improve to 10^{-7} with additional detector improvements [66].

To test for the existence of HNLs using **electron capture** measurements, total energy-momentum reconstruction of all non-neutrino final states is needed. Electron capture is a pure two body decay process, where the recoiling atom and the electron neutrino are the only final state particles, but additional energy is carried away by the de-excitation x-ray or auger electron. The energy-momentum conservation can be probed by measuring the atom and the associated de-excitation products. The mixing $|U_{e4}|^2$ can be probed by looking for a separated non-zero missing mass peak. The *BeEST* experiment has set limits at the 10^{-4} level in the 100 keV to 850 keV mass range, using berillium-7, which has a Q value of 862 keV. After planned upgrades to the experiment, the sensitivity is expected to improve to the 10^{-7} level [67].

Reactor searches up to 12 MeV in mass are possible at short baseline experiments using commercial or research reactors, which are a strong source of electron antineutrinos and could therefore also produce HNLs if $|U_{e4}|^2$ is non-zero. Visible decay channels at these energies are $\nu_4 \rightarrow \nu_e e^+ e^-$, $\nu_4 \rightarrow \nu \gamma$, and $\nu_4 \rightarrow \nu \gamma \gamma$, where the first dominates. The first analysis in this field, reports limits at the 10^{-4} level in the 2 MeV to 7 MeV mass range [68].

mention the Z boson decay results from DELPHI (because they are strong in $U_{\tau 4}$, too (RED))

[63]: Osipowicz et al. (2001), “KATRIN: A Next generation tritium beta decay experiment with sub-eV sensitivity for the electron neutrino mass. Letter of intent”

[64]: Mertens et al. (2019), “A novel detector system for KATRIN to search for keV-scale sterile neutrinos”

[65]: Aker et al. (2023), “Search for keV-scale sterile neutrinos with the first KATRIN data”

[66]: Abi et al. (2020), “Deep Underground Neutrino Experiment (DUNE), Far Detector Technical Design Report, Volume II: DUNE Physics”

[67]: Friedrich et al. (2021), “Limits on the Existence of sub-MeV Sterile Neutrinos from the Decay of ^7Be in Superconducting Quantum Sensors”

[68]: Hagner et al. (1995), “Experimental search for the neutrino decay $\nu_3 + \nu_j + e^+ + e^-$ and limits on neutrino mixing”

Atmospheric and Solar

Natural sources of neutrinos are provided up to 20 MeV by the sun and up to 100s of GeV by neutrino production in the atmosphere. Both fluxes contain all flavors of neutrinos, due to mixing and oscillations, and can therefore be used to directly probe the mixings with ν_e , ν_μ , and ν_τ . Depending on the HNL mass and the strength of the mixing, which both govern the decay length, different signatures can be used to experimentally access large regions of the HNL parameter space. The strength of the mixing defines the total rate of HNL events, which is additionally affected by whether solely the minimal mass mixing is assumed, or also more complicated mixing scenarios, like the dipole portal, are considered.

So far, only very few analyses exist, which are performed by the experimental collaborations themselves. Several external theoretical groups have predicted the expected sensitivities to HNLs, produced from solar or atmospheric neutrinos, based on various coupling scenarios and decay lengths. A selection of the potential analyses will be discussed in the following.

[39]: Bellini et al. (2013), “New limits on heavy sterile neutrino mixing in B8 decay obtained with the Borexino detector”

For very long-lived particles, **production inside the sun** can be used as a source to search for HNLs in detectors on earth. This will only allow production through non-zero $|U_{e4}|^2$, because the initial solar neutrino flux is only ν_e . By searching for HNL decays to a SM neutrino and an electron positron pair $\nu_4 \rightarrow \nu_e e^+ e^-$ and comparing to the expected inter planetary positron flux, *Borexino* has placed the strongest limits on the mixing $|U_{e4}|^2$ at the order of 10^{-5} in the few MeV mass range [39].

[62]: Plestid (2021), “Luminous solar neutrinos I: Dipole portals”

[69]: Plestid (2021), “Luminous solar neutrinos II: Mass-mixing portals”

For HNL decay length scales of the order of the Earth’s diameter, HNL **up-scattering outside the detector** is possible, where a neutrino from the solar or the atmospheric neutrino flux scatters in the Earth and transfers some kinetic energy into the mass of the HNL, which can then later decay inside the detector. For HNL masses below 18 MeV produced from solar neutrinos, (external) limits were derived using the Borexino data for purely tau coupling through mass mixing [62] and for all flavor coupling through the dipole portal [69]. At similar decay length scales, the HNL could also be produced directly in the atmosphere, but neither this channel, nor the production anywhere in the Earth from atmospheric neutrinos has been investigated yet.

[70]: Coloma et al. (2017), “Double-Cascade Events from New Physics in Icecube”

[71]: Coloma (2019), “Icecube/Deep-Core tests for novel explanations of the MiniBooNE anomaly”

[72]: Atkinson et al. (2022), “Heavy Neutrino Searches through Double-Bang Events at Super-Kamiokande, DUNE, and Hyper-Kamiokande”

[73]: Coloma et al. (2021), “GeV-scale neutrinos: interactions with mesons and DUNE sensitivity”

If the HNL decay lengths are sufficiently short, **production and decay in the detector** can happen and the observation of two vertices could be used to constrain the mixing parameters. In principle, this could be possible with any neutrino flavor produced in the sun or the atmosphere, but so far only theoretical studies have been performed for mass-mixing and dipole-portal couplings for the atmospheric neutrino detectors *IceCube* [70, 71] and *Super-K*, *Hyper-K*, and *Dune* [72, 73]. Due to the high complexity of these experiments, several simplified assumptions were made in the studies, which might not hold in reality, and the results should be taken with caution. For reliable sensitivity estimates and limits the collaborations should perform their own analyses.

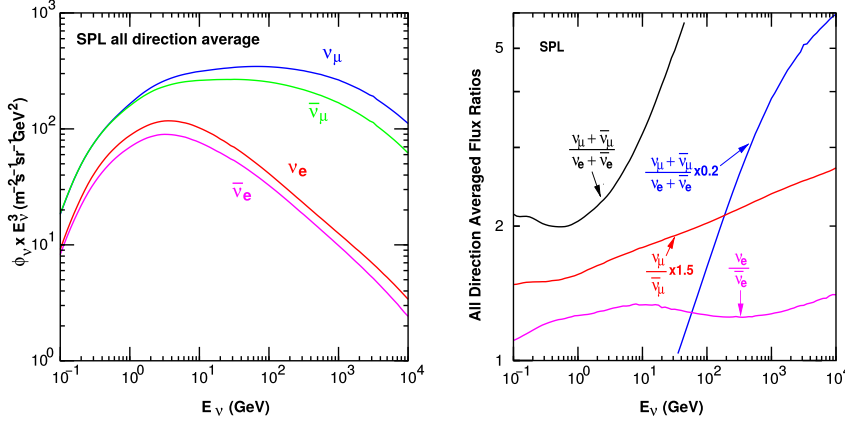


Figure 2.5: The atmospheric fluxes of different neutrino flavors as a function of energy (left) and the ratios between muon neutrinos and electron neutrinos as well as the ratios between neutrinos and antineutrinos for both those flavors (right). Results from the calculations performed for the geographic South Pole, taken from [75].

2.3 Atmospheric Neutrinos as Source of Heavy Neutral Leptons

This work focuses on the search for HNLs using atmospheric neutrinos as source for the production and decay inside the IceCube detector. The following sections will give a brief overview of the production of neutrinos in the atmosphere and the oscillations they undergo, before discussing the expected signatures of HNLs in the detector, where they are produced from the incoming neutrinos and subsequently decay.

2.3.1 Production of Neutrinos in the Atmosphere

The analysis performed in this work is based on the sample of neutrinos observed in IceCube DeepCore at energies below 100 GeV. At these energies, the flux exclusively originates in the Earth's atmosphere. Highly relativistic cosmic rays (protons and heavier nuclei [74]) interact in the upper atmosphere, producing showers of secondary particles. Neutrinos are produced in decays of charged Pions and Kaons (π and K mesons) present in those showers, where the dominant contribution comes from the decay chain

$$\begin{aligned}\pi^\pm &\rightarrow \mu^\pm + \nu_\mu(\bar{\nu}_\mu), \\ \mu^\pm &\rightarrow e^\pm + \bar{\nu}_\mu(\nu_\mu) + \nu_e(\bar{\nu}_e),\end{aligned}\tag{2.22}$$

where muon neutrinos ν_μ and muons μ^\pm are produced in the first decay and both electron and muon neutrinos $\nu_{e/\mu}$ are produced in the second decay. Atmospheric muons, which are also produced in these decays, are the main background component for IceCube DeepCore analyses.

The different atmospheric flux components are shown in Figure 2.5 (left), for a much broader energy range than relevant for this work. Both neutrinos and antineutrino fluxes are shown for electron and muon neutrinos and all fluxes are the directionally averaged expectation calculated at the South Pole. Muon neutrinos are dominating the flux and from Equation 2.22 the naive assumption would be that the ratio between muon and electron neutrinos is $(\nu_\mu + \bar{\nu}_\mu)/(\nu_e + \bar{\nu}_e) = 2$. This is roughly true at energies below 1 GeV, where all muons decay in flight, but at larger energies muons can reach the detector before decaying, which increases the ratio to approximately 10:1 at around 100 GeV. Additionally, kaon decays start to contribute which also increases the number of muons and muon neutrinos. The increasing ratio can be seen

[74]: Tanabashi et al. (2018), "Review of Particle Physics"

in Figure 2.5 (right), which also shows the ration between neutrinos and antineutrinos for both flavors.

Charged mesons or tau particles can also be produced in cosmic ray interactions. Their decays lead to the production of tau neutrinos. At the energies relevant for this work however, the resulting tau neutrino flux is negligible as compared to the muon neutrino flux [76] and is not considered in the analysis. This is because both charged mesons and tau particles are much heavier than Pions and Kaons and therefore their production is suppressed at high energies.

[76]: Fedynitch et al. (2015), “Calculation of conventional and prompt lepton fluxes at very high energy”

Say something about atmospheric neutrino flux uncertainties, based on recent JP/Anatoli papers. (YELLOW)

2.3.2 Neutrino Oscillations

Describing neutrinos in their mass state as introduced in Section ?? is crucial to understand their propagation through space and time and to explain neutrino oscillations. Oscillations mean that a neutrino changes from its initial flavor, that it was produced with, to another flavor and back after traveling a certain distance.

The neutrino propagation in vacuum can be expressed by applying a plane wave approach, where the mass eigenstates evolve as

$$|v_k(t)\rangle = e^{-iE_k t/\hbar} |v_k\rangle . \quad (2.23)$$

The energy of the mass eigenstate $|v_k\rangle$ is $E_k = \sqrt{\vec{p}^2 c^2 + m_k^2 c^4}$, with momentum \vec{p} and mass m_k , \hbar is the reduced Planck constant, and c is the speed of light in vacuum. A neutrino is produced as a flavor eigenstate $|v_\alpha\rangle$ in a CC weak interaction, but its propagation happens as the individual mass states it is composed of. The probability of finding the neutrino with initial flavor $|v_\alpha\rangle$ in the flavor state $|v_\beta\rangle$ after the time t is calculated as

$$P_{v_\alpha \rightarrow v_\beta}(t) = |\langle v_\beta | v_\alpha(t) \rangle|^2 , \quad (2.24)$$

[77]: Dirac (1927), “The Quantum Theory of the Emission and Absorption of Radiation”

by applying Fermi’s Golden Rule [77], which defines the transition rate from one eigenstate to another by the strength of the coupling between them. This coupling strength is the square of the matrix element and using the fact that the mixing matrix is unitary ($U^{-1} = U^\dagger$) to describe the mass eigenstates as flavor eigenstates, we find the time evolution of the flavor state $|v_\alpha(t)\rangle$, which can be inserted into Equation 2.24 to find the probability as

$$P_{v_\alpha \rightarrow v_\beta}(t) = \sum_{j,k} U_{\beta j}^* U_{\alpha j} U_{\beta k} U_{\alpha k}^* e^{-i(E_k - E_j)t/\hbar} . \quad (2.25)$$

The indices j and k run over the mass eigenstates.

We can approximate the energy as

$$E_k \approx E + \frac{c^4 m_k^2}{2E} \longrightarrow E_k - E_j \approx \frac{c^4 \Delta m_{kj}^2}{2E} , \quad (2.26)$$

for small neutrino masses compared to their kinetic energy. Here, $\Delta m_{kj}^2 = m_k^2 - m_j^2$ is the mass-squared splitting between states k and j . Replacing the time in Equation 2.25 by the distance traveled by relativistic neutrinos

$t \approx L/c$ we get

$$P_{\nu_\alpha \rightarrow \nu_\beta}(t) = \delta_{\alpha\beta} - 4 \sum_{j>k} \text{Re}(U_{\beta j}^* U_{\alpha j} U_{\beta k} U_{\alpha k}^*) \sin^2\left(\frac{c^3 \Delta m_{kj}^2}{4E\hbar} L\right) + 2 \sum_{j>k} \text{Im}(U_{\beta j}^* U_{\alpha j} U_{\beta k} U_{\alpha k}^*) \sin^2\left(\frac{c^3 \Delta m_{kj}^2}{4E\hbar} L\right), \quad (2.27)$$

which is called the survival probability if $\alpha = \beta$, and the transition probability if $\alpha \neq \beta$. Once again, this probability is only non-zero if there are neutrino mass eigenstates with masses greater than zero. Additionally, there must be a mass-squared difference Δm^2 and non-zero mixing between the states. Since we assumed propagation in vacuum in Equation 2.23, the transition and survival probabilities correspond to vacuum mixing.

The mixing matrix can be parameterized as [74]

$$U = \begin{pmatrix} 1 & 0 & 0 \\ 0 & c_{23} & s_{23} \\ 0 & -s_{23} & c_{23} \end{pmatrix} \begin{pmatrix} c_{13} & 0 & s_{13}e^{-i\delta_{CP}} \\ 0 & 1 & 0 \\ -s_{13}e^{i\delta_{CP}} & 0 & c_{13} \end{pmatrix} \begin{pmatrix} c_{12} & s_{12} & 0 \\ -s_{12} & c_{12} & 0 \\ 0 & 0 & 1 \end{pmatrix}, \quad (2.28)$$

where $c_{ij} = \cos \theta_{ij}$ and $s_{ij} = \sin \theta_{ij}$ are cosine and sine of the mixing angle θ_{ij} , that defines the strength of the mixing between the mass eigenstates i and j , and δ_{CP} is the neutrino CP-violating phase. Experiments are sensitive to different mixing parameters, depending on the observed energy range, neutrino flavor, and the distance between the source and the detector L , commonly referred to as *baseline*. To be able to resolve oscillations the argument

$$\frac{\Delta m^2 L}{4E} \quad (2.29)$$

should be at the order of 1. This divides experiments into ones that are sensitive to very slow oscillations from $\Delta m_{21}^2 \approx \mathcal{O}(10^{-5} \text{eV}^2)$ and ones that are sensitive to faster oscillations from $\Delta m_{31}^2 \approx \mathcal{O}(10^{-3} \text{eV}^2)$. Relevant for this work are the parameters that can be measured at the earth's surface using atmospheric neutrinos, which are Δm_{31}^2 , θ_{23} , and θ_{13} , because the flux is primarily composed of muon neutrinos and antineutrinos. Applying the parameterization from Equation 2.28 to Equation 2.27 and using the fact that θ_{13} is small and θ_{12} is close to $\pi/4$, the survival probability of muon neutrinos can be approximated as

$$P_{\nu_\mu \rightarrow \nu_\mu} \simeq 1 - 4|U_{\mu 3}|^2(1 - |U_{\mu 3}|^2) \sin^2\left(\frac{\Delta m_{31}^2 L}{4E}\right) \simeq 1 - \sin^2(2\theta_{23}) \sin^2\left(\frac{\Delta m_{31}^2 L}{4E}\right), \quad (2.30)$$

while the tau neutrino appearance probability is

$$P_{\nu_\mu \rightarrow \nu_\tau} \simeq 4|U_{\mu 3}|^2|U_{\tau 3}|^2 \sin^2\left(\frac{\Delta m_{31}^2 L}{4E}\right) \simeq \sin^2(2\theta_{23}) \sin^2\left(\frac{\Delta m_{31}^2 L}{4E}\right). \quad (2.31)$$

The latest global fit [78] of all the parameters is shown in Table 2.2.

[74]: Tanabashi et al. (2018), "Review of Particle Physics"

Parameter	Global Fit
θ_{12} [°]	$33.41^{+0.75}_{-0.72}$
θ_{13} [°]	$8.54^{+0.11}_{-0.12}$
θ_{23} [°]	$49.1^{+1.0}_{-1.3}$
Δm_{21}^2 [10^{-5}eV^2]	$7.41^{+0.21}_{-0.20}$
Δm_{31}^2 [10^{-3}eV^2]	$2.511^{+0.028}_{-0.027}$
δ_{CP} [°]	197^{+42}_{-25}

Table 2.2: Results from the latest global fit of neutrino mixing parameters from [78].

[78]: Esteban et al. (2020), "The fate of hints: updated global analysis of three-flavor neutrino oscillations"

say something about matter effect? (ORANGE)

say something about mass ordering? (ORANGE)

2.3.3 Neutrino Interactions with Nuclei

The neutrino detection principle of IceCube DeepCore is explained in Chapter ?? and relies on the weak interaction processes between neutrinos and the nuclei of the Antarctic glacial ice. At neutrino energies above 5 GeV, the cross-sections are dominated by *deep inelastic scattering (DIS)*, where the neutrino is energetic enough to resolve the underlying structure of the nucleons and interact with one of the composing quarks individually. As a result the nucleon breaks and a shower of hadronic secondary particles is produced. Depending on the type of interaction, the neutrino either remains in the final state for NC interactions or is converted into its charged lepton counterpart for CC interactions. The CC DIS interactions have the form

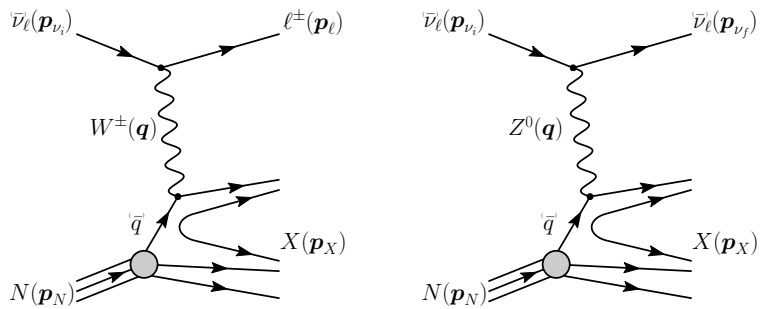
$$\begin{aligned} \nu_l + N &\rightarrow l^- + X, \\ \bar{\nu}_l + N &\rightarrow l^+ + X, \end{aligned} \quad (2.32)$$

where $\nu_l/\bar{\nu}_l$ and l^-/l^+ are the neutrino/antineutrino and its corresponding lepton/antilepton, and l can be either an electron, muon, or tau. N is the nucleon and X stands for any set of final state hadrons. The NC DIS interactions are

$$\begin{aligned} \nu_l + N &\rightarrow \nu_l + X \text{ and} \\ \bar{\nu}_l + N &\rightarrow \bar{\nu}_l + X. \end{aligned} \quad (2.33)$$

Figure 2.6 shows the Feynman diagrams for both processes DIS interactions

Figure 2.6: Feynman diagrams for deep inelastic scattering of a neutrino with a nucleon via charged-current (left) and neutral current (right) interactions. p_{ν_i} , p_N and p_{ν_f} , p_l , p_N are the input and output four-momenta, while q is the momentum transfer. Taken from [79].



have a roughly linear energy dependent cross-section above ~ 20 GeV and are well measured and easy to theoretically calculate. They are the primary interaction channel for neutrinos detected with IceCube.

At energies below 5 GeV, *quasi-elastic scattering (QE)* and *resonant scattering (RES)* become important. At these energies the neutrinos interact with the approximately point-like nucleons, without breaking them up in the process. RES describes the process of a neutrino scattering off a nucleon producing an excited state of the nucleon in addition to a charged lepton. It is the dominant process at 1.5 GeV to 5 GeV for neutrinos and 1.5 GeV to 8 GeV for antineutrinos. Below 1.5 GeV QE is the main process, where protons are converted to neutrons in antineutrino interactions and vice-versa for neutrino interactions. Additionally, a charged lepton corresponding to the neutrino/antineutrino flavor is produced. The cross-sections of QE and RES scattering processes are not linear in energy and the transition region from QE/RES to DIS is poorly understood. The total cross-sections and their composition is shown in Figure 2.7. It can be seen that the interaction cross-sections are very small at the order of 10^{-38} cm^2 . This is the reason why very

large volume detectors are required to measure atmospheric neutrinos with sufficient statistics to perform precision measurements of their properties. The interaction length of a neutrino with $E_\nu = 10$ GeV is of $\mathcal{O}(10 \times 10^{10} \text{ km})$, for example.

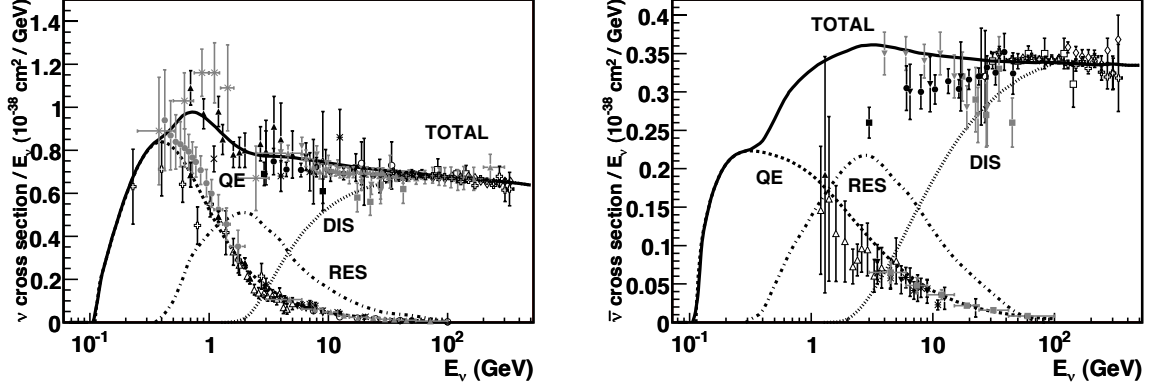


Figure 2.7: Total neutrino (left) and antineutrino (right) per nucleon cross-section divided by neutrino energy plotted against energy. The three main scattering processes quasi-elastic scattering (QE), resonant scattering (RES), and deep-inelastic scattering (DIS) are shown. Taken from [80].

2.3.4 Heavy Neutral Lepton Production and Decay

For the search conducted in this work, both production and decay are assumed to happen inside the detector, therefore probing decay lengths ranges at the scale of the detector size, which is below 1000 m. Since the mixing with the first two generations of leptons is already strongly constrained as was discussed in Section 2.3, only the mixing with the tau neutrino will be considered in the following. Due to the effect of oscillations, described in Section 2.3.2, the initial atmospheric muon neutrino flux provides a sizable tau neutrino flux at the detector.

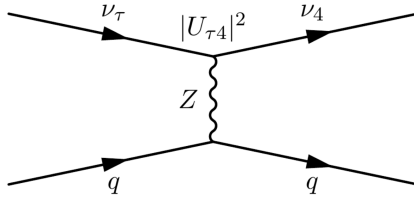


Figure 2.8: Feynman diagram of the HNL production. The heavy mass state is produced in the up-scattering of a tau neutrino.

For a non-zero $|U_{\tau 4}|^2$, the HNL can be produced through **up-scattering in the ice**. An incoming tau neutrinos scatters on an ice nucleus and transfers some of its kinetic energy to the heavy neutrino. The Feynman diagram of this process is shown in Figure 2.8. The custom NC cross-sections calculated for this purpose are explained in more detail in Section ??, but are similar to the SM tau neutrino NC cross-sections, with a reduction scaling with the mixing $|U_{\tau 4}|^2$ and energy dependent reductions, due to kinematic constraints because of the heavy neutrino mass. The scattering process produces a hadronic cascade, which will produce light in the detector.

After a certain distance, the HNL will **decay in the ice**, where the possible decay channels considered in this work are shown in Figure 2.9 and the underlying, explicit calculations are discussed in Section ?. The decay can be a CC or NC and both purely leptonic and leptonic+mesonic modes

Figure 2.9: Decay widths of the HNL within the mass range considered, calculated based on the results from [73]. Given the existing constraints on $|U_{e4}|^2$ and $|U_{\mu 4}|^2$, we consider that the corresponding decay modes are negligible.

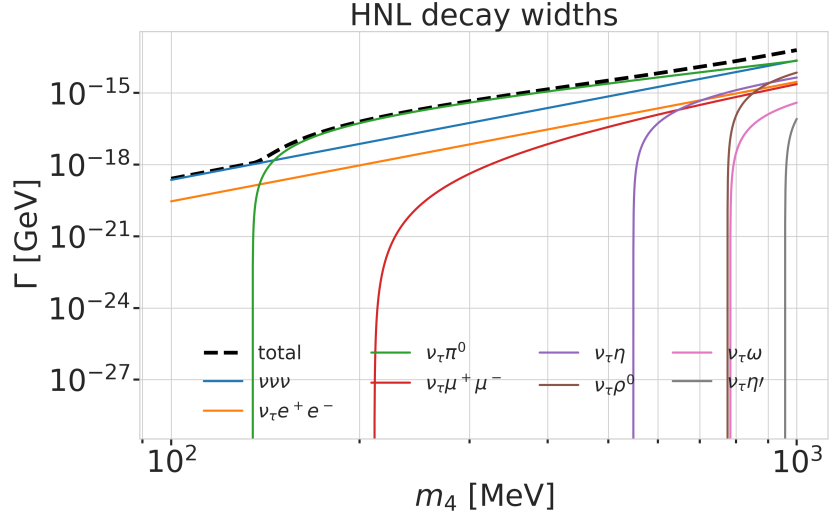
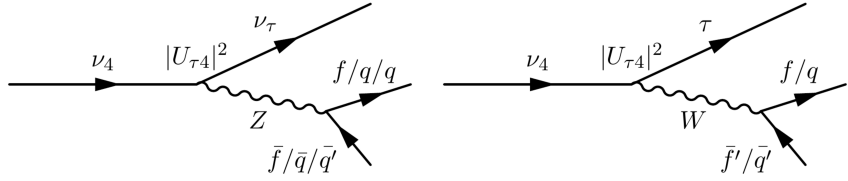


Figure 2.10: Feynman diagram of the HNL decay. The heavy mass state can decay through neutral current interaction (left) into a tau neutrino and a charged lepton or quark pair, or through charged current interaction (right) into a tau lepton and a charged lepton or quark.



are possible. The Feynman diagrams of the decays can be seen in Section ?? . Only the mass range relevant for this work is presented and mixing with $\nu_{e/\mu}$ is assumed to be negligible. Depending on the decay channel, an electromagnetic or a hadronic cascade is produced, while some energy is carried away by the invisible neutrino. The decay length of the HNL is defined by its proper lifetime¹, which is given by

$$\tau_{\text{proper}} = \frac{\hbar}{\Gamma_{\text{total}}(m_4) \cdot |U_{\tau 4}|^2}, \quad (2.34)$$

where \hbar is the reduced Planck constant, $\Gamma_{\text{total}}(m_4)$ is the total decay width of the HNL for the given mass, and $|U_{\tau 4}|^2$ is the mixing with the tau neutrino. The total decay width is the sum of the partial decay widths for all possible decay channels. The mean lab frame decay length is then given by

$$L_{\text{decay}} = \gamma v \tau_{\text{proper}}, \quad (2.35)$$

where γ is the Lorentz factor of the HNL, defined by the kinetic energy. This will be further discussed on Section ?? . Figure 2.11 shows the mean decay lengths for an example mass of $m_4 = 0.6 \text{ GeV}$ and several mixing values.

1: A particle decay time follows an exponential distribution, with mean lifetime given by the proper lifetime. The proper lifetime is the lifetime in the rest frame of the particle.

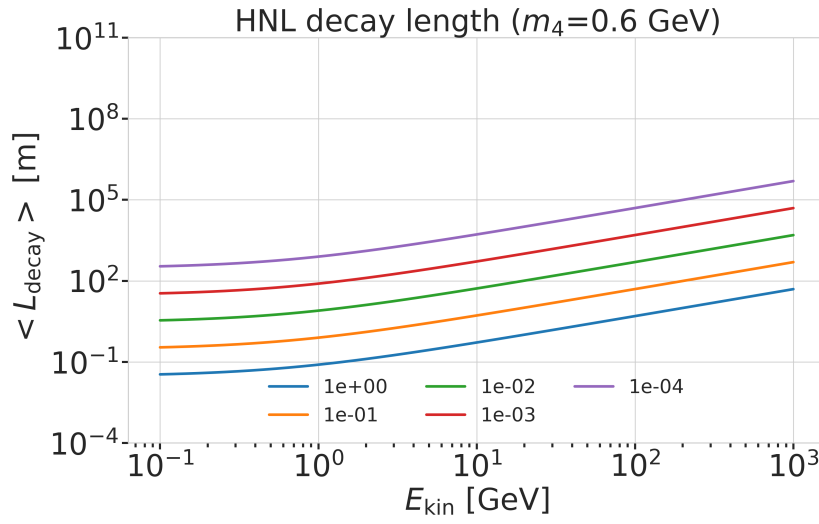


Figure 2.11: Theoretical mean decay length of the HNL for a mass of 0.6 GeV and different mixing values.

Standard Model Background Simulation and Data Processing

3

The analysis presented in this thesis is highly dependent on an efficient event selection to reduce the raw IceCube trigger data to a usable atmospheric neutrino sample. Based on this selection, a precise estimation of both expected SM background and expected BSM signal events can be made using MC simulations. This chapter describes the current simulation and event selection chain used for state-of-the-art IceCube neutrino oscillation measurements like [81]. The whole chain can be broadly split into 4 steps:

Step 1 Event Generation: The initial step for all particle (non-noise) simulation is the generation of events from selected initial distributions and fluxes. Events are the primary particle and the particles produced in the interaction with the ice.

Step 2 Detector Simulation: The particles from the first step are propagated through the ice, producing Cherenkov photons, which are then propagated further until they reach a DOM or are absorbed. If they hit a DOM the detector response (acceptance and PMT) is simulated.

Step 3 Processing: Starting from the PMT output, both real data and simulation are processed through the in-ice trigger, the online filter and processing, and the low energy event selection to produce a neutrino dominated sample.

Step 4 Reconstruction: Once the sample is small enough for more sophisticated reconstruction techniques to be feasible to run, the events are reconstructed using a CNN and some high level variables are computed. Based on these variables the final event selection is applied.

This chapter only describes the event generation for the SM background simulation (neutrinos and muons), while the signal simulation is described in Chapter ???. The detector simulation is identical for both signal and background events while processing and reconstruction are applied to all simulation and data in the same way. Splitting the simulation steps has the advantage of reusing the outputs of for example the generation step to propagate the particles with different ice model, in order to estimate the systematic impacts of uncertainties of the ice properties. Similar approach can be taken for varying detector response and through this a more efficient (reduced) use of computing resources can be achieved. The following sections describe the different steps in more detail and the last section, Section 3.5, describes the related systematic uncertainties considered for this work.

3.1 Event Generation

The MC is used in the analysis by applying a method called *forward folding*, where a very large number of events (signal and background) is produced using sampling distribution that are tuned to have a large selection efficiency. Those distributions don't have to be physically correct distributions, but they need to cover the full parameter space of interest for the analysis. To produce a physical distribution, the events are weighted given a specific

Adapt chapter to reflect
switched chapter order
(RED)

3.1	Event Generation . . .	23
3.2	Detector Simulation . . .	25
3.3	Processing	27
3.4	Reconstruction	31
3.5	Systematic Uncertain- ties	33

[81]: Abbasi et al. (2023), "Measure-
ment of atmospheric neutrino mix-
ing with improved IceCube Deep-
Core calibration and data process-
ing"

Table 3.1: Cylinder volumes used for GENIE neutrino simulation generation. Cylinder is always centered in DeepCore at $(x, y, z) = (46.29, -34.88, -330.00)$ m.

Flavor	Energy [GeV]	Radius [m]	Length [m]	Events/File	Files
$\nu_e + \bar{\nu}_e$	1-4	250	500	450000	650
	4-12			100000	
	12-100	350	600	57500	
	100-10000	550	1000	6700	
$\nu_\mu + \bar{\nu}_\mu$	1-5	250	500	440000	1550
	5-80	400	900	57500	
	80-1000	450	1500	200000	
	1000-10000	550	1500	26000	
$\nu_\tau + \bar{\nu}_\tau$	1-4	250	500	1500000	350
	4-10			300000	
	10-50	350	600	375000	
	50-1000	450	800	200000	
	1000-10000	550	1500	26000	

choice of physics and nuisance parameters. The large number of raw MC events ensures a good estimation of the expected numbers and weighted distributions.

The analysis itself is then performed by comparing the weighted MC distributions to the observed data. This is done by binning them as described in Chapter ?? and calculating a loss function comparing the bin expectations to the data. The physics and nuisance parameters that best correspond to the observed data are estimated by minimizing this loss function. In order to achieve a reliable result with this method the MC needs to be precise and as close to the data as possible (at least at the final event selection).

3.1.1 Neutrinos

Due to the very low interaction rate of neutrinos, the event generation is performed in a way that forces every event to interact in a chosen sampling volume. The weight of each event is then calculated as the inverse of the simulated neutrino fluence

$$w_{\text{gen}} = \frac{1}{F_{\text{sim}}} \frac{1}{N_{\text{sim}}} , \quad (3.1)$$

where F_{sim} is the number of neutrino events per energy, time, area, and solid angle and N_{sim} is the number of simulated events. If this weight is multiplied by the livetime and the theoretically expected neutrino flux for a given physical model, it results in the number of expected events in the detector for this particular MC event. The baseline neutrino flux used in this thesis, computed for the South Pole, is taken from Honda *et al.* [75].

The simulation volume is a cylinder centered in DeepCore with radius and height chosen such that all events possibly producing a signal are contained. The different sizes, chosen depending on energy and neutrino flavor, are shown in Table 3.1. The directions of the neutrinos are sampled isotropically and the energies are sampled from an E^{-2} power law. The number of simulated events is chosen such that the livetime is more than 70 years for each flavor. Neutrinos and antineutrinos are simulated with ratios of 70% and 30%, respectively.

[75]: Honda et al. (2015), “Atmospheric neutrino flux calculation using the NRLMSISE-00 atmospheric model”

To simulate the neutrino interaction with the ice, the GENIE event generator [82] (version 2.12.8) is used, resulting in the secondary particles and the kinematic and cross-section parameters. As input, the outdated GRV98LO [83] *parton distribution functions* (PDFs) was used, because it was the only option that could incorporate extrapolations to lower Q^2 [84]. Muons produced in these interactions are propagated using PROPOSAL [85], also simulating their Cherenkov light output. The shower development of gamma rays, electrons, and positrons below 100 MeV and hadronic showers below 30 GeV is simulated using Geant4 [86] while for higher energies an analytical approximation from [87] is used.

3.1.2 Muons

Atmospheric muons are generated on a cylinder surface enclosing the full IceCube detector array. The cylinder has a height of 1600 m and a radius of 800 m. The energy is sampled from an E^{-3} power law while the other sampling distributions (position, direction) are found from parameterizations based on [88]. This work uses full CORSIKA [89] simulations of muons to tailor the parameterizations, starting from *cosmic ray* (CR) interactions with atmospheric nuclei using the CR flux model from [90] and producing the muons applying the *hadronic interaction* (HI) model SIBYLL 2.1 [91]. After the generation, they are propagated through the ice with PROPOSAL producing photons, treating them exactly like the muons produced in neutrino interactions.

Since the offline processing and selection steps described in Section 3.3.2 and Section 3.4 reduce the muon contamination to an almost negligible level, the statistical uncertainty on the number of expected muon events at the final selection level is large and therefore two separate sets of muon simulation are produced. A **first set** including all events resulting from the above described generation to tune the lower level selection (up to L4) and a **second set** to estimate the muon contamination at higher levels (above L5), which only accepts muon events if they pass through a smaller cylinder centered in DeepCore (height of 400 m and radius of 180 m) and rejects events based on a KDE estimated muon density at L5 (in energy and zenith) increasing the simulation efficiency at L5 significantly .

[82]: Andreopoulos et al. (2015), "The GENIE Neutrino Monte Carlo Generator: Physics and User Manual"

[83]: Glück et al. (1998), "Dynamical parton distributions revisited"

[84]: Bodek et al. (2003), "Higher twist, $\xi(\omega)$ scaling, and effective LO PDFs for lepton scattering in the few GeV region"

[85]: Koehne et al. (2013), "PROPOSAL: A tool for propagation of charged leptons"

[86]: Agostinelli et al. (2003), "Geant4—a simulation toolkit"

[87]: Rädle et al. (2012), "Calculation of the Cherenkov light yield from low energetic secondary particles accompanying high-energy muons in ice and water with Geant4 simulations"

[88]: Becherini et al. (2006), "A parameterisation of single and multiple muons in the deep water or ice"

[89]: Heck et al. (1998), "CORSIKA: A Monte Carlo code to simulate extensive air showers"

[90]: Gaisser (2012), "Spectrum of cosmic-ray nucleons, kaon production, and the atmospheric muon charge ratio"

[91]: Engel et al. (2017), "The hadronic interaction model Sibyll – past, present and future"

put a number on this significant increase? (YELLOW)

3.2 Detector Simulation

The detector simulation is performed after the event generation, where the initial particles and the resulting photons and secondary particles from their propagation were produced. This part of the simulation chain is applied to all muon and neutrino simulation as well as the HNL signal simulation explained in detail in Chapter ?? . The detector simulation can be split into two parts, the propagation of the photons and the simulation of the detector response (including internal noise).

3.2.1 Photon Propagation

Any photon that was produced in the event generation is individually traced through the ice, simulating scattering and absorption processes. The

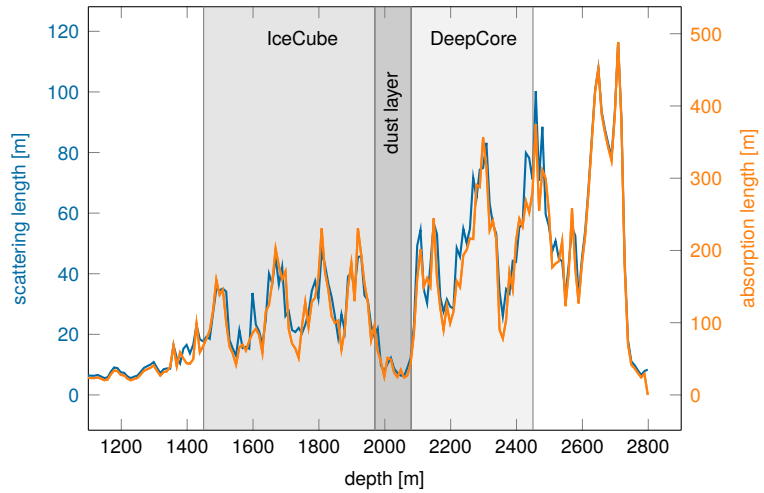


Figure 3.1: Scattering and absorption lengths in the SPICE model used for simulation production as a function of depth, modified from [19].

[93]: Chirkin et al. (2019), “Photon Propagation using GPUs by the IceCube Neutrino Observatory”

[94]: Aartsen et al. (2013), “Measurement of South Pole ice transparency with the IceCube LED calibration system”

put a number on the tilt angle? (YELLOW)

propagation is done using `CLSIM` [92] which is an implementation of the *Photon Propagation Code (PPC)* [93] in `OPENCL`. It is optimized to be run very efficiently on GPUs, which is what is done for IceCube simulation production. The ice is modeled as a set of 10 m thick, almost horizontal layers with specific absorption and scattering lengths. The *South Pole ice (SPICE)* model [94] accounts for the layers being tilted by a small amount () and the absorption and scattering lengths having a non-uniformity with respect to the azimuth direction. Figure 3.1 shows the values of this model for the different depths, indicating the location of IceCube, DeepCore, and the dust layer.

In an initial step, each photon’s absorption length is sampled from an exponential distribution with the expectation value at the current layer’s absorption length. The following propagation steps are performed in parallel for all photons. In each of those steps, corresponding to a single scattering event, the photon travels a length that is sampled from an exponential distribution with the expectation value at the scattering length of the current layer and the scattering angle chosen based on a combination of a simplified Mie scattering distribution [95] and a Henyey-Greenstein distribution [96]. The parameters defining the shape of these distributions were calibrated using data from *in-situ* LED calibration runs. These steps are continuously repeated until each photon reached a DOM or was absorbed¹. After all photons have been propagated in that manner, the final step is to output the photons that reached a DOM for further processing.

[95]: Mie (1908), “Beiträge zur Optik trüber Medien, speziell kolloidaler Metallösungen”

[96]: Henyey et al. (1941), “Diffuse radiation in the Galaxy.”

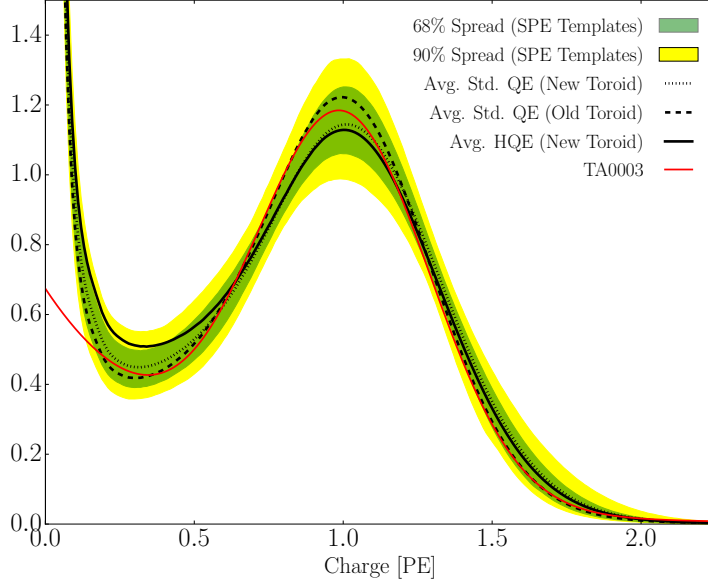
1: A photon is absorbed, when it traveled its full absorption length, sampled in the initial step of the photon propagation.

3.2.2 Detector Responses

The second part of simulating the IceCube detector is the DOM response. Whether a photon that reached a DOM produces a signal depends on the total efficiency and the angular acceptance curve of the specific DOM. The total efficiency includes effects of the DOM glass, PMT quantum and photo-electron collection efficiencies, and it is wavelength dependent. Additionally, there is another angle dependent effect called *hole ice* [97]. This effect is due to varied ice properties resulting from the re-freezing process of the water column inside the borehole after deployment of the string. Accepted photons are converted into a so-called *Monte Carlo photo-electron (MCPE)*. The amount of charge measured for each MCPE is determined by sampling

[97]: Fiedlschuster (2019), “The Effect of Hole Ice on the Propagation and Detection of Light in IceCube”

from a mixture of two exponential distributions and a normal distribution. This *single photo-electron (SPE)* distribution was tuned to match the observed distribution in each DOM in an *in-situ* calibration study [98]. Figure 3.2 shows the distribution compared to a lab measurement. Based on the sampled charges and times of MCPs, the voltage waveforms for the (two) different readout channels are simulated and passed on to the trigger simulation starting with *WaveDeform*, which was already mentioned in Section ??.



[98]: Aartsen et al. (2020), “In-situ calibration of the single-photoelectron charge response of the IceCube photomultiplier tubes”

Parameter	Value
Therm. rate λ_{th}	180 Hz
Decay rate λ_{dec}	80 Hz
Decay hits η	8.5
Decay μ	$4.3 \log_{10}(\text{ns})$
Decay σ	$1.8 \log_{10}(\text{ns})$

Table 3.2: Typical parameter values used in the *vuvuzela* noise simulation. Averaged over all DOMs.

Figure 3.2: Single photo-electron charge distribution shown for a lab measurement in red (TA0003), various hardware configurations in black dashed, dotted, and solid lines, and the 68 % and 90 % spread of the measured charged templates for all DOMs. All curves are normalized to the same area. The figure is taken from [98].

Besides the Cherenkov photons, IceCube also observes photons that are produced in radioactive decays inside the DOMs, both in the glass housing sphere and the PMT glass itself. To simulate this internal noise, the *Vuvuzela* module [99, 100] is used to create additional MCPs that are fed into the same simulation chain described above. This module takes into account thermal and non-thermal components and their times are sampled using parameterizations of the measured distributions, where the thermal noise component is uncorrelated photons and the non-thermal component is from burst of photons. The noise hits are simulated by drawing the times from a constant rate Poisson process and the number of photons from a Poisson distribution. Then the time differences between the individual photons per hit is found, based on a Log-Normal distribution. The simulation is defined by 5 parameters that are calibrated for each DOM individually. Table 3.2 shows the average values for these parameters.

3.3 Processing

After the detector simulation is performed, all MC and data are processed in exactly the same way. This section explains the trigger and event selection that is applied starting from the raw voltage measured by the PMTs. Most parts of this processing are identical to the procedure already described in [19, 101]. It is split in different steps run inside the ice, at the South Pole, and after the data was transferred to the North. The complexity and computational cost of the processing increases with each step, while the total number of

[99]: Larson (2013), “Simulation and Identification of Non-Poissonian Noise Triggers in the IceCube Neutrino Detector”

[100]: Larson (2018), “A Search for Tau Neutrino Appearance with IceCube-DeepCore”

[19]: Trettin (2023), “Search for eV-scale sterile neutrinos with IceCube DeepCore”

[101]: Lohfink (2023), “Testing non-standard neutrino interaction parameters with IceCube-DeepCore”

events reduces, making it feasible and reducing the use of computational resources on events that are not of interest for the analysis.

3.3.1 Trigger and Filter

Before the data can be sent to the North, the initial signal coming from the PMT is a voltage waveform that has to be digitized (for data) and then information of photon hits has to be extracted (also for the MC coming from the detector response simulation). The trigger and filter explained here are tailored to select events that passed through the DeepCore volume, while rejecting background events (either from atmospheric muons or from random noise). There are other filters used in IceCube which will not be explained here, since they are not relevant for this work. A full description of the instrumentation and the online systems can be found in [102].

[102]: Aartsen et al. (2017), “The IceCube Neutrino Observatory: Instrumentation and Online Systems”

Include some low level plots like the trigger efficiency for the HNL simulation (ORANGE)

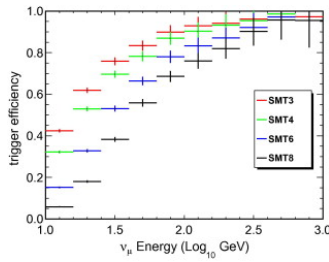


Figure 3.3: Efficiencies of different IceCube and DeepCore triggers, taken from [103].

[104]: Abbasi et al. (2009), “The IceCube data acquisition system: Signal capture, digitization, and timestamping”

[6]: Aartsen et al. (2017), “The IceCube Neutrino Observatory: instrumentation and online systems”

[103]: Abbasi et al. (2012), “The design and performance of IceCube DeepCore”

2: Where *online* means running on hardware at the South Pole.

In-ice Trigger

The trigger is applied inside the DOM in the ice before sending the information to the ICL on the surface. The time dependent voltage curves are captured if a pre-defined threshold value is exceeded. Once the threshold set to the equivalent of 0.25 PE is crossed, 6.4 μ s of the waveform are coarsely digitized by a *Fast Analog-to-Digital Converter (FADC)* with a sampling rate of 40 MHz. Additionally, the first 427 ns are digitized using an *Analog Transient Waveform Recorder (ATWD)* with a sampling rate of 300 MHz [104], but only if some trigger condition is met, because this readout frequency is too high to be sampled directly and requires some buffering. For DeepCore, the HLC condition already mentioned in Section ?? has to be met for three DOMs inside the fiducial volume within a time window of 5 μ s. If this is the case, all waveforms that crossed the threshold within a 20 μ s time window around the trigger are digitized and sent to the ICL for further processing. This trigger is called *Simple Multiplicity Trigger 3 (SMT-3)*. The DOM hits that are read out in this process, but do not meet the HLC condition, are called *soft local coincidence (SLC)* hits. The rate of the DeepCore SMT-3 trigger is ~ 250 Hz [6], accepting $\sim 70\%$ of ν_μ -CC events at 10 GeV and $\sim 90\%$ at 100 GeV [103]. The trigger efficiencies for different SMT triggers, including the DeepCore SMT-3, are shown in Figure 3.3.

Online Filter

The digitized waveforms are sent to the ICL, where a further filter is applied *online*². First, the WaveDeform algorithm is run to extract photon arrival times and charge from the waveforms, then the DeepCore filter is applied, which is an iterative hit cleaning starting from HLC hits and removing any hits outside a 125 m radius and a 500 ns time window (called *radius-time cleaning (RT-cleaning)*) of the initial hit. This mainly rejects unphysical SLC hits, which are potentially caused by random noise. The following selection steps are done using the resulting cleaned pulses.

Next, an additional cut is applied to reject events that are likely to be caused by atmospheric muons. This is done by splitting the hits depending on whether they were inside the DeepCore fiducial volume or outside and then calculating the speed of each hit outside the fiducial volume towards the

center of gravity (COG) of the hits inside. If one of them has a speed close to the speed of light, the whole event is rejected, because this is a strong indication for a muon event.

As input for the further selection levels, a few event properties, like vertex position and direction, are determined using fast and simple event reconstructions. After the DeepCore online filter, the rate is about 15 Hz, which can be sent to the North via satellite for further processing.

3.3.2 Event Selection

After the data was sent to the North, the *offline* filters and selection are applied to further reduce the background of atmospheric muons and noise. The selection is split into three levels referred to as *Level 3-5 (L3-L5)*, which bring down the neutrino and muon rate to ~ 1 mHz, while the remaining fraction of random noise is below 1 %.

Level 3

At the first offline filtering level, Level 3, 1D cuts are used to reduce atmospheric muons, pure noise, and coincident muons. These cuts are targeting regions where the data/MC agreement is poor, so that more sophisticated *machine learning (ML)* techniques can be applied at later levels. The cuts are made using 12 control variables, that are inexpensive to compute for the very large sample at this stage. The variables are related to position, time, and overall number of hits in the event.

Pure noise hits, that are temporally uncorrelated, are cleaned by applying a 300 ns sliding window, requiring the containment of more than 2 hits at its maximum. Additionally, an algorithm is run to check whether the hits show some directionality, accepting them only if they do.

To reduce the amount of muons a series of cuts is applied using spatial and temporal information. Events that have more than 9 hits observed above -200 m or the first HLC hit above -120 m are rejected as well as events where the fraction of hits in the first 600 ns of the event is above 0.37, ignoring the first two hit DOMs. Additionally, the ratio between hits in the veto region and the DeepCore fiducial volume is required to be below 1.5.

If a muon enters the detector after the data acquisition was already triggered, it causes events that span over a much larger time range. To reduce those coincident events, the time difference between first and last pulse cannot be above 5000 ns. This cut mainly affects a region of very poor data to MC agreement, because coincident events are not simulated at all.

The L3 cuts remove 95 % of the atmospheric muons and >99 % of pure noise hits, while keeping >60 % of the neutrino events. The sample now roughly contains muons/neutrinos/noise at a ratio of 100:10:1 with a total rate of ~ 0.5 Hz.

add example plots (??)
for L3 cut variables and
applied cuts (YELLOW)

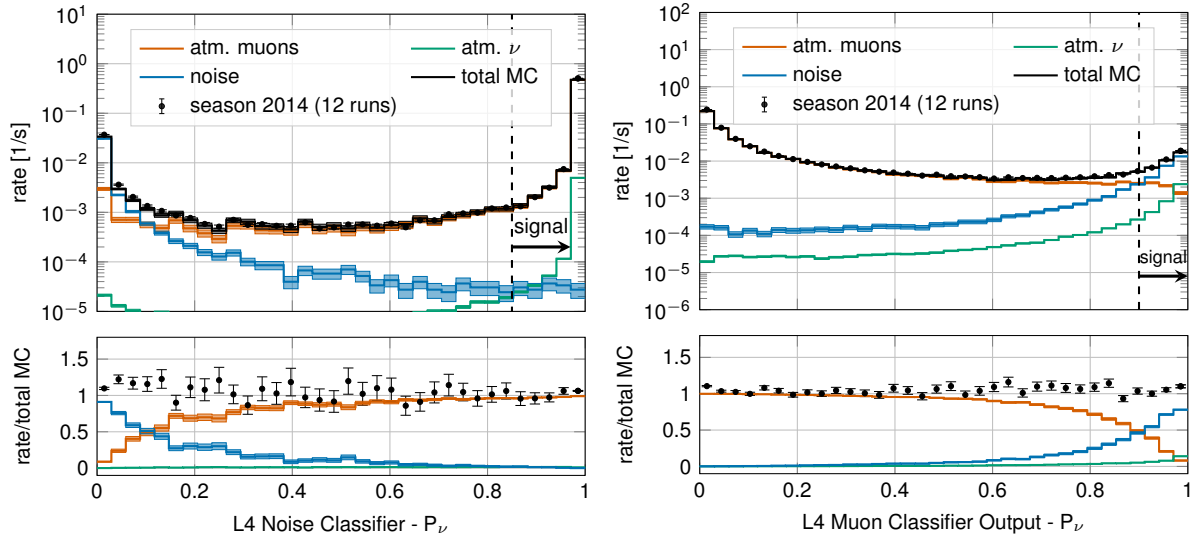


Figure 3.4: Distributions of Level 4 noise classifier output (left) and muon classifier output (right), where larger values indicate more neutrino-like and lower values more noise-like/muon-like. Taken from [81].

Level 4

[105]: Friedman (2002), “Stochastic gradient boosting”

After the total rate was reduced by the simple cuts of L3 and the overall agreement between data and MC is established, ML techniques can be applied to further reduce the background. For Level 4, two *Boosted Decision Trees (BDTs)* [105] classifier are trained to separate neutrino events from atmospheric muons and noise hits, separately. The output of each classifier, a probability score, can be seen in Figure 3.4. The noise filter is applied first and an event passes the score if it is larger than 0.7, reducing the noise hits by a factor of 100, while keeping 96 % of neutrinos. Then the second BDT classifier is applied to reject muons. It was trained partly on unfiltered data, which consists of >99 % atmospheric muons, to reject the data and keeping the neutrinos from the simulation. Rejecting events with a score smaller than 0.65 removes 94 % of atmospheric muons while keeping 87 % of neutrinos. This fraction varies depending on the flavor and interaction type, ν_μ -CC events for example, which have a muon in the final state, are therefore reduced to 82.5 %. After applying the L4 cuts based on the BDT classifier outputs, the sample is still dominated by atmospheric muons, while the noise rate dropped to below most neutrino types.

Level 5

Level 5 is the final selection level, before event reconstructions are applied. This level aims to reduce the remaining atmospheric muon rate below the rate of neutrinos. Muons not rejected by the earlier levels are those that produced little or no light in the veto regions. One possible reason is that they passed through one of the un-instrumented regions between the strings called *corridors*. To reject those, special corridor cuts, based on the number of hits they produced close to a potential corridor they passed through. The potential corridor in questions is identified based on a simple infinite track fit. In addition to the corridor cuts, starting containment cuts are applied to reject events that start at the edge of the fiducial volume. Events with more than seven hits in the outermost strings of the detector or those that have

add some figure showing the corridors? (YELLOW)

a down going direction in the uppermost region are rejected. This further reduces the fraction of muons by 96 % while keeping 48 % of neutrinos. The rates after this level are 1 mHz and 2 mHz for neutrinos and muons, respectively, making it a neutrino dominated sample.

3.4 Reconstruction

In the energy range most relevant for this work, between 10 GeV and 100 GeV, the light deposition is very low and only a few DOMs detect light, making the reconstructions difficult. In [106] two classical methods are described, which have partly been applied in one recent IceCube atmospheric neutrino oscillation measurement using a sub-sample of the DeepCore sample [81]. The algorithm used in this work on the other hand, is a newer method that applies a *convolutional neural network (CNN)* to reconstruct the events and determine some discriminating quantities. The latest muon neutrino disappearance result from IceCube [107] is based on this reconstruction.

3.4.1 Fast Low Energy Reconstruction using Convolutional Neural Networks

As the name *Fast Low Energy Reconstruction using Convolutional Neural Networks (FLERCNN)* already indicates, the FLERCNN reconstruction [108, 109] is a CNN optimized to reconstruct IceCube events at low energies (<100 GeV) in a fast and efficient manner, by leveraging the approximate translational invariance of event patterns within the detector. The architecture of the network is very similar to the preexisting IceCube CNN event reconstruction [110], but optimized on low energy events and specifically tailored to include the DeepCore sub-array. Only the eight DeepCore strings and the central 19 IceCube strings are used for the reconstruction (compare to Figure ??). Because of the different z-positions of the DeepCore and IceCube DOMs, they are divided into two networks that are combined in the final layer of the network. The full architecture is shown in Figure 3.5. The first dimension of the network is the string index, while the second dimension is the order of the DOMs along the vertical axis. The horizontal position of the DOMs is not used, since the strings are arranged in an irregular pattern. The information from the DOM hits is summarized into five charge and time variables, which make up the last dimension of the input layer. The variables are the total summed charge, the time of the first hit, the charge weighted mean time of the hits, the time of the last hit, and the charge weighted standard deviation of the hit times.

Five different networks are trained using this architecture. Three networks do the regression of the events' energy, zenith angle, and the starting vertex (x, y, z position), while two of them are used for classification. One is trained to predict the probability of the event being a track (used as PID) and the other to predict the probability of the event being a muon. Each network is trained with an MC sample modified to have a flat distribution in the target variable, to be unbiased for that variable and ideally extending outside the target reconstruction region. For the classification tasks the loss function is the *binary cross entropy* and the activation function is a *sigmoid*. To perform the regression of zenith and vertex position, the loss function is the *mean*

add table with rates per level (split in flavor) - maybe better in analysis chapter to also show signal? (RED)

[106]: Abbasi et al. (2022), "Low energy event reconstruction in IceCube DeepCore"

[81]: Abbasi et al. (2023), "Measurement of atmospheric neutrino mixing with improved IceCube DeepCore calibration and data processing"

[107]: Yu et al. (2023), "Recent neutrino oscillation result with the IceCube experiment"

[108]: Yu et al. (2021), "Direction reconstruction using a CNN for GeV-scale neutrinos in IceCube"

[109]: Micallef (),

[110]: Huennefeld (2017), "Deep Learning in Physics exemplified by the Reconstruction of Muon-Neutrino Events in IceCube"

add image with selected strings used for flercnn IC and DC (YELLOW)

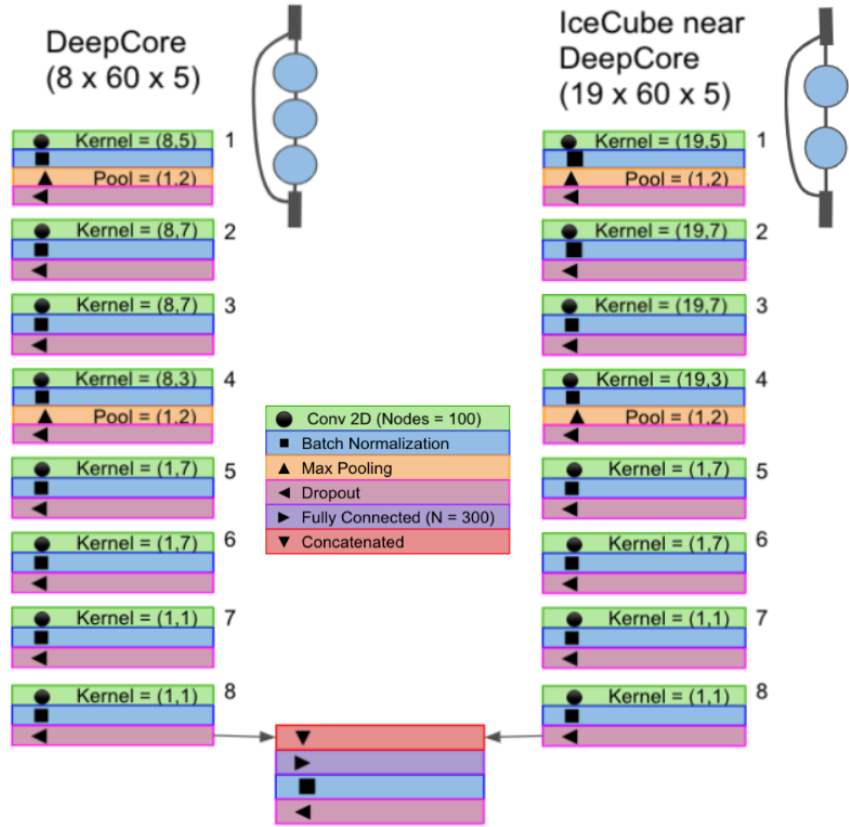


Figure 3.5: Architecture of the FLERCNN neural networks, taken from [108].

add some performance plots of the FLERCNN reconstruction (ORANGE)

There is more information on pre-processing the samples and preparing the input features, and training each cnn, but I'm not sure if that might be too much detail? (YELLOW)

3: A radial variable that is often used in IceCube, is the horizontal distance to string 36 called ρ_{36} , which is basically the distance to the center of IceCube.

add reference for flercnn analysis internal note (ORANGE)

squared error (MSE), while for the energy it is the *mean absolute percentage error*. The activation for all regression tasks is *linear*.

3.4.2 Analysis Selection

Before the reconstruction is applied a few additional high level variables are computed, which are from fast and inexpensive algorithms. Then the reconstruction is performed by applying the trained FLERCNN networks to get the output quantities. After that, another BDT classifier is trained to further reduce the muon background for the final sample. The BDT is trained on five high level variables, where three are FLERCNN reconstruction variables (vertex z , ρ_{36}^3 , and muon probability) and two are lower level variables (L4 muon classifier output and L5 corridor cut variable). To train the BDT, the FLERCNN nominal simulation set is used, only using events with $\cos(\theta_{zenith}) \leq 0.3$. The output of the BDT is the neutrino probability and a cut at 0.8 is applied to reject events with a high probability of being a muon. Figure 3.6 shows the output of the BDT classifier, where the neutrinos in both training and testing sets are gathered at 1 and muons are around 0, which shows great classification power.

To get the final, pure sample of well reconstructed neutrinos another set of cuts is applied. The first cuts are meant to reject events with poor reconstruction quality, by requiring the events to fall into the DeepCore volume, where the denser, better instrumented detector leads to enhanced resolution. The cuts are applied on the vertex z and ρ_{36} and are listed in Table 3.3. The FLERCNN reconstruction was optimized for atmospheric neutrino analyses which are mainly in the region below 100 GeV and there

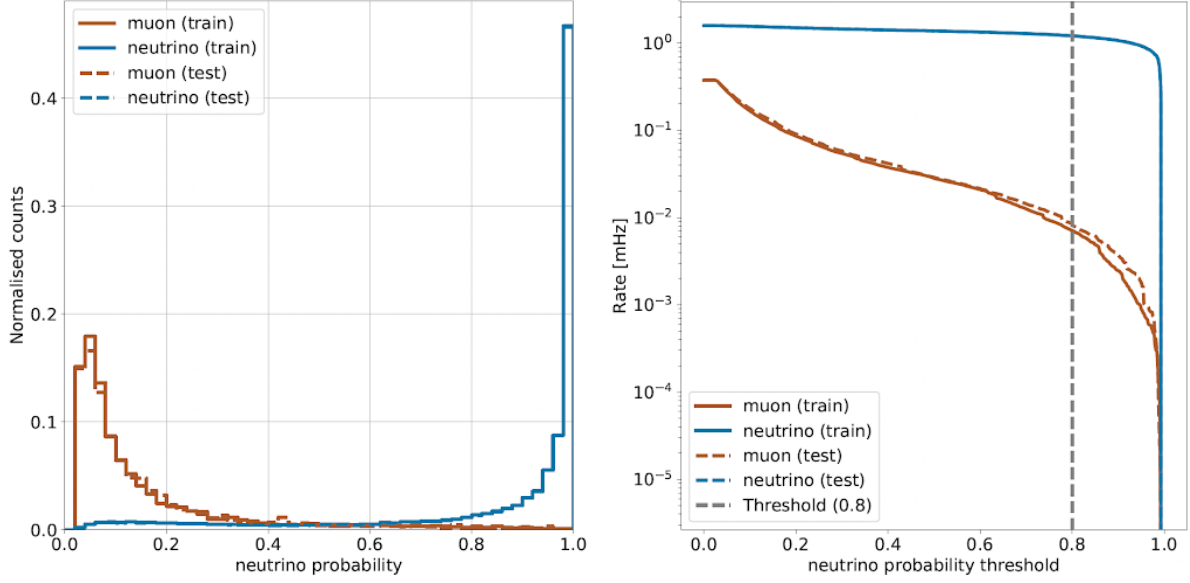


Figure 3.6: FLERCNN muon classifier output score (left) and rate of neutrinos and muons as function of muon classifier cut (right). Taken from [flercnn_analysis_internal_note]

Variable	Threshold	Removed
Number of hit DOMs	≥ 7	1.05 %
Radial distance	< 200 m	0.09 %
Vertical position	$-495 \text{ m} < z < -225 \text{ m}$	5.48 %
Energy	$5 \text{ GeV} < E < 100 \text{ GeV}$	20.70 %
Cosine of zenith angle	< 0.04	19.66 %
Number of direct hits	> 2.5	10.50 %
Number of hits in top layers	< 0.5	0.03 %
Number of hits in outer layer	< 7.5	0.001 %
Muon classifier score	≥ 0.8	23.90 %

Table 3.3: Cuts performed to select the final analysis sample. Parts of the cuts are meant to increase the data/MC agreement, while others are meant to reject events with poor reconstruction quality.

are very few events with energies below 5 GeV, so the reconstructed energy is required to be in that range. Additionally, rejecting events with fewer than seven hits in the selected DOMs used for FLERCNN showed to increase the resolution.

Another set of cuts is applied to make sure the agreement between data and MC is good. To remove coincident muon and neutrino events, cuts are applied to the number of hits in the top 15 layers of IceCube DOMs and the number of hits in the outermost IceCube strings. Coincident random noise events are removed by requiring more than three hit DOMs from direct photons⁴. Neither of the two coincident event types are simulated, which can be seen as bad agreement between data and MC. The last cut is on the reconstructed cosine zenith, which is required to be smaller than 0.04 to reject down-going muons.

4: *Direct photons* are photons that were not scattered on their way from the interaction vertex to the DOM.

3.5 Systematic Uncertainties

There are multiple sources of systematic uncertainties related to the event generation and processing explained in this chapter. All uncertainties considered in this work need to be implemented with parameters that can be varied continuously so that a simultaneous fit of the physics and systematic

parameters can be performed. Where possible, a correct model of the effect is used, but in many cases the variations are captured by effective parameters. Uncertainties that solely scale the total event rate are not included individually, since the analysis only uses the relative distribution of events and a single scaling parameter N_ν is used to scale the total neutrino rate instead.

3.5.1 Atmospheric Flux Uncertainties

The flux of atmospheric neutrinos is influenced by multiple factors, the spectrum and composition of CRs, the assumed atmospheric conditions, and the HI model used to describe the air showers development. Uncertainties of the neutrino flux are therefore dictated by the uncertainties on these components, where the variations in atmospheric conditions were found to have negligible effect [81].

[81]: Abbasi et al. (2023), “Measurement of atmospheric neutrino mixing with improved IceCube DeepCore calibration and data processing”

[111]: Dembinski et al. (2017), “Data-driven model of the cosmic-ray flux and mass composition from 10 GeV to 10^{11} GeV”

[112]: Barr et al. (2006), “Uncertainties in atmospheric neutrino fluxes”

[113]: Evans et al. (2017), “Uncertainties in atmospheric muon-neutrino fluxes arising from cosmic-ray primaries”

[81]: Abbasi et al. (2023), “Measurement of atmospheric neutrino mixing with improved IceCube DeepCore calibration and data processing”

Cosmic ray flux: The selected sample of atmospheric neutrinos lies around energies of up to 100 GeV. The initial primary particles in the CR flux can have 100 times larger energies and therefore the CR flux between 10 GeV and 10 TeV is important, which dominantly consists of hydrogen and helium nuclei [111]. The uncertainty in this CR flux component can be described as a power law correction [112, 113]

$$\Phi'_\nu = \Phi_\nu \left(\frac{E}{E^\star} \right)^{\Delta\gamma}, \quad (3.2)$$

where E^\star is the pivot energy and $\Delta\gamma$ is the correction to the power law exponent. This modification propagates into the neutrino flux, which is therefore corrected in the same way. E^\star was chosen to be 24 GeV as to minimize the dependence of the overall flux scale on $\Delta\gamma$ [81].

Hadronic interaction model: Neutrinos are produced in the decaying hadrons in CR air showers, spanning a large parameter space that is sparsely evaluated by experimental data. To include uncertainties based on energy, direction, and neutrino flavor, the MCEQ package [114] is used to compute the distribution of atmospheric leptons and to estimate the impact of varying their contributions. The calculations result in the change in flux $d\Phi_1/dB$ for a variation dB of some parameter B . Scaling this variation by some value b , the modified total flux, s is then given by

$$\Phi'_1 = \Phi_1 + \left(b \cdot \frac{d\Phi_1}{dB} \right). \quad (3.3)$$

[115]: Barr et al. (2006), “Uncertainties in Atmospheric Neutrino Fluxes”

[116]: Riehn et al. (2020), “Hadronic interaction model sibyll 2.3d and extensive air showers”

[111]: Dembinski et al. (2017), “Data-driven model of the cosmic-ray flux and mass composition from 10 GeV to 10^{11} GeV”

5: The choice of flux and HI model have minor impact on the variations.

Matching the work in [115], the parameter space is divided in regions of the primary energy, E_i , and the energy fraction of the secondary meson, x_{lab} , with varying uncertainties, derived from fixed target experiment data. The Sibyll2.3c [116] HI model and the GSF CR flux [111] were used to calculate the related flux changes⁵ for the different regions in E_i and x_{lab} , resulting in 17 variables, encoding the possible changes. Figure 3.7 shows the selected regions of the parameter space and the names given to the uncertainties. The variational term in Equation 3.3 is applied for each of these parameters and the total variation is the sum of all individual variations.

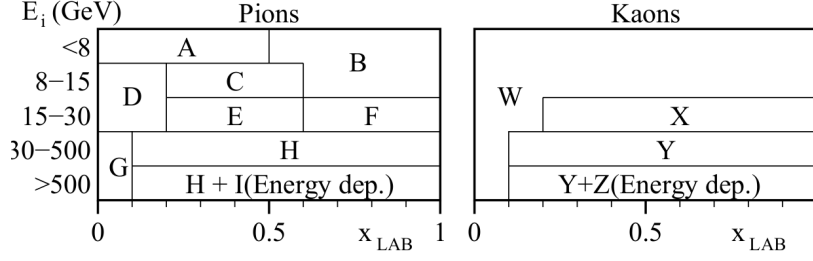


Figure 3.7: Flux uncertainty regions of the hadronic interaction model in the phase space of the primary energy E_i and the energy fraction of the secondary meson x_{lab} . Taken from [115].

3.5.2 Cross-Section Uncertainties

The uncertainties related to the cross-sections are split into low and high energy components, since there is no coherent model to explain both DIS interactions, which are the dominant processes above 20 GeV, and *charged current resonance production (CCRES)* and *charged current quasi elastic scattering (CCQE)*, which are relevant below 20 GeV where interactions with the nucleons as a whole are important. Three parameters are included to account for all relevant cross-sections uncertainties.

At low energies two parameters are included accounting for uncertainties in form factors of CCQE and CCRES events. These uncertainties are due to uncertainties in the *axial mass* M_A , which enters the form factor as in

$$F(Q^2) \sim \frac{1}{(1 - (\frac{Q}{M_A})^2)^2}, \quad (3.4)$$

where Q^2 is the momentum transfer squared. The axial mass can be determined experimentally and to include uncertainties on the values of M_A^{CCQE} and M_A^{CCRES} , the cross-sections are computed with GENIE, where the form factors are calculated varying the axial mass by $\pm 20\%(1\sigma)/\pm 40\%(1\sigma)$ around the nominal value. This is an approximation of the recommended uncertainties by the GENIE collaboration, which are -15% , $+25\%$ for M_A^{CCQE} and $\pm 20\%$ for M_A^{CCRES} [82]. To apply a continuous uncertainty variation of the axial mass in a fit, the total cross-section is fit with a quadratic function to interpolate between the cross-sections computed with the different axial masses.

which experiments measure the axial mass? (ORANGE)

Even though the DIS interactions can be calculated very precisely, there are still uncertainties in the input PDF, describing the probability of finding a specific parton (quark) with a specific momentum fraction x inside a nucleon. To account for differences between the used method and more sophisticated methods using newer PDFs seen at high energies, an uncertainty parameter is introduced. The parameter is based on the discrepancy between the cross-sections computed with GENIE and the ones computed with CSMS [117] above 100 GeV. The included parameter scales the cross-section from the GENIE values to the CSMS values, which are considered more accurate above 100 GeV. The scaling is done as a function of energy and inelasticity and to guarantee continuity, the scaling is extrapolated linearly below 100 GeV. The parameter is designed such that a value of 0.0 corresponds to the GENIE cross-sections and a value of 1.0 gives an approximation of the CSMS cross-sections. A comparison of the total cross-sections GENIE (scaled/unscaled) with the data is shown in Figure 3.8.

[117]: Cooper-Sarkar et al. (2011), “The high energy neutrino cross-section in the Standard Model and its uncertainty”

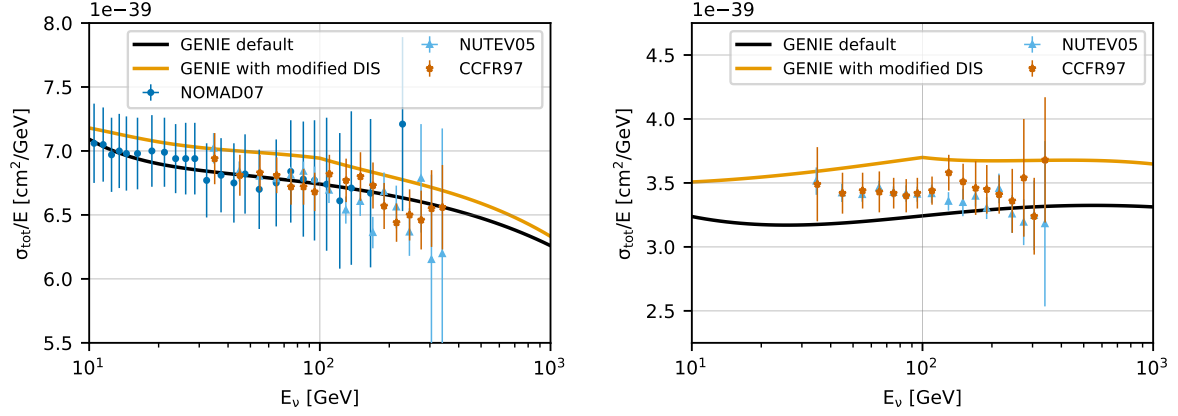


Figure 3.8: Inclusive total neutrino-nucleon cross-sections on an isoscalar target (black) for neutrinos (left) and antineutrinos (right) calculated with GENIE, comparing to measurements from NOMAD [118], NUTEV [119], and CCFR [120]. The scaled GENIE cross-section (orange) is also shown. Taken from [81].

3.5.3 Detector Calibration Uncertainties

The detection process of neutrinos in IceCube has several sources of uncertainties, where the effects of the properties of the ice itself and the optical efficiency of the DOMs are dominant for this analysis. None of these uncertainties can be described by an analytic expression, so they have to be estimated using MC simulation. This is done by producing additional systematic simulation samples at discrete values of those parameters. The five relevant uncertainty parameters are the absolute efficiency of the DOMs, a global scaling of bulk ice scattering and absorption lengths, and variations of the relative angular acceptance due to hole ice variations in two parameters. To perform the fit, continuous variations with respect to these parameters, will be derived with a method explained in Section ??.

DOM efficiency: As was already mentioned in Section ??, the absolute efficiency of the DOMs, ϵ_{DOM} is calibrated using minimum ionizing muons from air showers, due to the lack of a calibrated light source in the detector. Using the muons as a steady, controlled source of light, the efficiency can be estimated by comparing simulated muon data sets with varied DOM response to the measured data. Since the uncertainties found in multiple iterations of this study [121, 122] are at the order of 10 %, this systematic is highly relevant and has to be included in the analysis.

[121]: Feintzeig (2014), “Searches for Point-like Sources of Astrophysical Neutrinos with the IceCube Neutrino Observatory”

[122]: Kulacz (2019), “In Situ Measurement of the IceCube DOM Efficiency Factor Using Atmospheric Minimum Ionizing Muons”

Bulk ice scattering and absorption: Absorption and scattering length are the most important properties that govern the propagation of photons through the ice. The simulation principle and how the depth dependent absorption and scattering coefficients are used was already explained in Section 3.2.1. To account for uncertainties on this model of the bulk ice coefficients, a global scaling for each of the two parameters (global absorption, global scattering) is applied.

Hole ice angular acceptance: Due to bubble formation in the re-freezing process of the boreholes, the hole ice seems to be less transparent in the center of the columns [123]. This effectively decreases the chance of pho-

[123]: Rongen, Martin (2016), “Measuring the optical properties of IceCube drill holes”

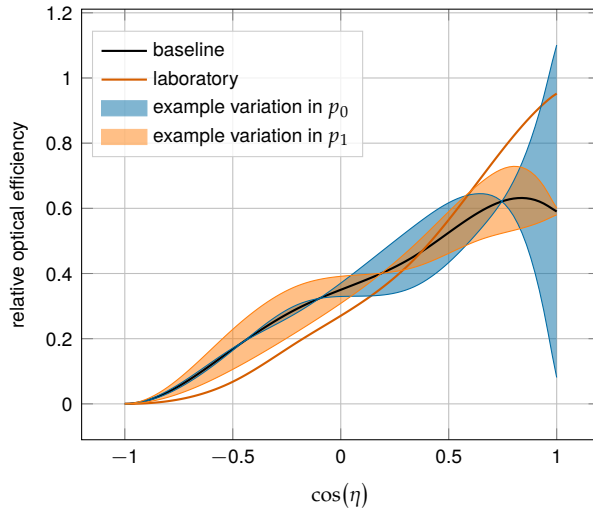


Figure 3.9: Relative angular acceptance modification due to hole ice. Shown is the current baseline model, the variations from changing p_0 and p_1 , and a laboratory measurement. Modified from [19].

tons hitting the DOMs directly from below, which can be described as an additional angular modification of the DOM acceptance. The modification is parameterized by a two dimensional, normalized⁶ function, where the two dominant of the parameters (p_0, p_1), dictating its form, are enough to describe all past and the current hole ice models from both *in-situ* and laboratory measurements. Figure 3.9 shows the acceptance modification as a function of the incident photon angle $\cos(\eta)$. The current baseline model, the variations achieved through modifying p_0 and p_1 , and a laboratory measurement can be seen.

6: The hole ice angular acceptance modification is normalized so that it does not affect the total charge.

Ice Model: The ice model used in IceCube is continuously improved, and the recent models incorporate the birefringent polycrystalline microstructure [124] into the bulk ice properties. To account for the uncertainty, due to this un-modeled effect in the ice model used for the simulation production, an additional simulation sample is produced using the newer version of the ice model, that incorporates the *birefringence* (BFR) effect.

[124]: Abbasi et al. (2024), “In situ estimation of ice crystal properties at the South Pole using LED calibration data from the IceCube Neutrino Observatory”

3.5.4 Muon Uncertainties

The muon fraction in the final level selection (see Section 3.4.2) is below 1 %, therefore additional muon systematic uncertainties apart from the spectral index are not implemented, but rather a total muon scaling parameter is added. This total scale is somewhat degenerate with the DOM efficiency, since an increased DOM efficiency leads to better muon rejection. Both the total muon scaling and the muon spectral index have a very small impact on the analysis as will be shown in Section ??.

cite this? (YELLOW)

List of Figures

2.1	Feynman diagrams of neutrino weak interactions	7
2.2	Current leading $ U_{e4}^2 - m_4$ limits	11
2.3	Current leading $ U_{\mu 4}^2 - m_4$ limits	12
2.4	Current leading $ U_{\tau 4}^2 - m_4$ limits	13
2.5	Atmospheric neutrino fluxes	15
2.6	Neutrino-nucleon deep inelastic scattering	18
2.7	Total inclusive neutrino-nucleon cross-sections	19
2.8	Feynman diagram of heavy neutral lepton production	19
2.9	HNL decay widths	20
2.10	Feynman diagram of heavy neutral lepton decay	20
2.11	Theoretical mean HNL decay length (0.6 GeV mass)	21
3.1	Depth dependent scattering and absorption lengths	26
3.2	Single photo-electron charge distribution	27
3.3	IceCube trigger efficiencies	28
3.4	Level 4 classifier outputs (muon and noise)	30
3.5	FLERCNN architecture	32
3.6	FLERCNN muon classifier probability distributions	33
3.7	Hadronic model flux uncertainty regions in hadron phase space	35
3.8	Inclusive total neutrino-nucleon cross-sections	36
3.9	Hole ice angular acceptance modification	37

List of Tables

2.1	Standard model fermions	6
2.2	Global fit neutrino mixing parameter results	17
3.1	GENIE generation cylinder volumes	24
3.2	Vuvuzela noise simulation parameters	27
3.3	Final analysis cuts	33

Bibliography

Here are the references in citation order.

- [1] W. Pauli. “Dear radioactive ladies and gentlemen”. In: *Phys. Today* 31N9 (1978), p. 27 (cited on page 2).
- [2] C. L. Cowan et al. “Detection of the Free Neutrino: a Confirmation”. In: *Science* 124.3212 (1956), pp. 103–104. doi: [10.1126/science.124.3212.103](https://doi.org/10.1126/science.124.3212.103) (cited on page 2).
- [3] G. Danby et al. “Observation of High-Energy Neutrino Reactions and the Existence of Two Kinds of Neutrinos”. In: *Phys. Rev. Lett.* 9 (1 July 1962), pp. 36–44. doi: [10.1103/PhysRevLett.9.36](https://doi.org/10.1103/PhysRevLett.9.36) (cited on page 2).
- [4] K. Kodama et al. “Observation of tau neutrino interactions”. In: *Physics Letters B* 504.3 (2001), pp. 218–224. doi: [https://doi.org/10.1016/S0370-2693\(01\)00307-0](https://doi.org/10.1016/S0370-2693(01)00307-0) (cited on page 2).
- [5] R. Davis, D. S. Harmer, and K. C. Hoffman. “Search for Neutrinos from the Sun”. In: *Phys. Rev. Lett.* 20 (21 May 1968), pp. 1205–1209. doi: [10.1103/PhysRevLett.20.1205](https://doi.org/10.1103/PhysRevLett.20.1205) (cited on pages 2, 8).
- [6] M. G. Aartsen et al. “The IceCube Neutrino Observatory: instrumentation and online systems”. In: *Journal of Instrumentation* 12.3 (Mar. 2017), P03012. doi: [10.1088/1748-0221/12/03/P03012](https://doi.org/10.1088/1748-0221/12/03/P03012) (cited on pages 2, 28).
- [7] C. N. Yang and R. L. Mills. “Conservation of Isotopic Spin and Isotopic Gauge Invariance”. In: *Physical Review* 96.1 (Oct. 1954), pp. 191–195. doi: [10.1103/PhysRev.96.191](https://doi.org/10.1103/PhysRev.96.191) (cited on page 5).
- [8] S. Weinberg. “A Model of Leptons”. In: *Phys. Rev. Lett.* 19 (21 Nov. 1967), pp. 1264–1266. doi: [10.1103/PhysRevLett.19.1264](https://doi.org/10.1103/PhysRevLett.19.1264) (cited on page 5).
- [9] S. L. Glashow. “Partial-symmetries of weak interactions”. In: *Nuclear Physics* 22.4 (Feb. 1961), pp. 579–588. doi: [10.1016/0029-5582\(61\)90469-2](https://doi.org/10.1016/0029-5582(61)90469-2) (cited on page 5).
- [10] R. Jackiw. “Physical Formulations: Elementary Particle Theory. Relativistic Groups and Analyticity. Proceedings of the eighth Nobel Symposium, Aspenäsgråden, Lerum, Sweden, May 1968. Nils Svartholm, Ed. Interscience (Wiley), New York, and Almqvist and Wiksell, Stockholm, 1969. 400 pp., illus. \$31.75.” In: *Science* 168.3936 (1970), pp. 1196–1197. doi: [10.1126/science.168.3936.1196.b](https://doi.org/10.1126/science.168.3936.1196.b) (cited on page 5).
- [11] P. Higgs. “Broken symmetries, massless particles and gauge fields”. In: *Physics Letters* 12.2 (1964), pp. 132–133. doi: [https://doi.org/10.1016/0031-9163\(64\)91136-9](https://doi.org/10.1016/0031-9163(64)91136-9) (cited on page 5).
- [12] S. Chatrchyan et al. “Observation of a New Boson at a Mass of 125 GeV with the CMS Experiment at the LHC”. In: *Phys. Lett. B* 716 (2012), pp. 30–61. doi: [10.1016/j.physletb.2012.08.021](https://doi.org/10.1016/j.physletb.2012.08.021) (cited on page 5).
- [13] G. Aad et al. “Observation of a new particle in the search for the Standard Model Higgs boson with the ATLAS detector at the LHC”. In: *Phys. Lett. B* 716 (2012), pp. 1–29. doi: [10.1016/j.physletb.2012.08.020](https://doi.org/10.1016/j.physletb.2012.08.020) (cited on page 5).
- [14] M. Gell-Mann. “A Schematic Model of Baryons and Mesons”. In: *Resonance* 24 (1964), pp. 923–925 (cited on page 5).
- [15] G. Zweig. “An SU(3) model for strong interaction symmetry and its breaking. Version 2”. In: *DEVELOPMENTS IN THE QUARK THEORY OF HADRONS. VOL. 1. 1964 - 1978*. Ed. by D. B. Lichtenberg and S. P. Rosen. Feb. 1964, pp. 22–101 (cited on page 5).
- [16] D. J. Gross and F. Wilczek. “Ultraviolet Behavior of Non-Abelian Gauge Theories”. In: *PRL* 30.26 (June 1973), pp. 1343–1346. doi: [10.1103/PhysRevLett.30.1343](https://doi.org/10.1103/PhysRevLett.30.1343) (cited on page 5).
- [17] C. Giunti and C. W. Kim. *Fundamentals of Neutrino Physics and Astrophysics*. Oxford University Press, Mar. 2007 (cited on page 5).

- [18] M. D. Schwartz. *Quantum Field Theory and the Standard Model*. Cambridge University Press, 2013 (cited on page 5).
- [19] A. Trettin. “Search for eV-scale sterile neutrinos with IceCube DeepCore”. PhD thesis. Berlin, Germany: Humboldt-Universität zu Berlin, Mathematisch-Naturwissenschaftliche Fakultät, 2023. doi: <https://github.com/atrettin/PhD-Thesis> (cited on pages 7, 10, 26, 27, 37).
- [20] N. Deruelle, J.-P. Uzan, and P. de Forcrand-Millard. *Relativity in Modern Physics*. Oxford University Press, Aug. 2018 (cited on page 8).
- [21] R. L. Workman et al. “Review of Particle Physics”. In: *Progress of Theoretical and Experimental Physics* 2022.8 (Aug. 2022), p. 083C01. doi: [10.1093/ptep/ptac097](https://doi.org/10.1093/ptep/ptac097) (cited on page 8).
- [22] M. Fukugita and T. Yanagida. “Baryogenesis without grand unification”. In: *Physics Letters B* 174.1 (1986), pp. 45–47. doi: [https://doi.org/10.1016/0370-2693\(86\)91126-3](https://doi.org/10.1016/0370-2693(86)91126-3) (cited on page 8).
- [23] Y. Fukuda et al. “Evidence for Oscillation of Atmospheric Neutrinos”. In: *Phys. Rev. Lett.* 81 (8 Aug. 1998), pp. 1562–1567. doi: [10.1103/PhysRevLett.81.1562](https://doi.org/10.1103/PhysRevLett.81.1562) (cited on page 8).
- [24] Q. R. Ahmad and other. “Direct Evidence for Neutrino Flavor Transformation from Neutral-Current Interactions in the Sudbury Neutrino Observatory”. In: *Phys. Rev. Lett.* 89 (1 June 2002), p. 011301. doi: [10.1103/PhysRevLett.89.011301](https://doi.org/10.1103/PhysRevLett.89.011301) (cited on page 8).
- [25] S. Alam et al. “Completed SDSS-IV extended Baryon Oscillation Spectroscopic Survey: Cosmological implications from two decades of spectroscopic surveys at the Apache Point Observatory”. In: *Phys. Rev. D* 103 (8 Apr. 2021), p. 083533. doi: [10.1103/PhysRevD.103.083533](https://doi.org/10.1103/PhysRevD.103.083533) (cited on page 8).
- [26] N. Aghanim et al. “Planck2018 results: VI. Cosmological parameters”. In: *Astronomy & Astrophysics* 641 (Sept. 2020), A6. doi: [10.1051/0004-6361/201833910](https://doi.org/10.1051/0004-6361/201833910) (cited on page 8).
- [27] M. Aker et al. “Direct neutrino-mass measurement with sub-electronvolt sensitivity”. In: *Nature Phys.* 18.2 (2022), pp. 160–166. doi: [10.1038/s41567-021-01463-1](https://doi.org/10.1038/s41567-021-01463-1) (cited on page 8).
- [28] T. Asaka, S. Blanchet, and M. Shaposhnikov. “The nuMSM, dark matter and neutrino masses”. In: *Phys. Lett. B* 631 (2005), pp. 151–156. doi: [10.1016/j.physletb.2005.09.070](https://doi.org/10.1016/j.physletb.2005.09.070) (cited on page 10).
- [29] T. Asaka and M. Shaposhnikov. “The ν MSM, dark matter and baryon asymmetry of the universe”. In: *Phys. Lett. B* 620 (2005), pp. 17–26. doi: [10.1016/j.physletb.2005.06.020](https://doi.org/10.1016/j.physletb.2005.06.020) (cited on page 10).
- [30] P. Minkowski. “ $\mu \rightarrow e \gamma$ at a rate of one out of 10^9 muon decays?” In: *Physics Letters B* 67.4 (Apr. 1977), pp. 421–428. doi: [10.1016/0370-2693\(77\)90435-X](https://doi.org/10.1016/0370-2693(77)90435-X) (cited on page 10).
- [31] T. Yanagida. “Horizontal Symmetry and Masses of Neutrinos”. In: *Progress of Theoretical Physics* 64.3 (Sept. 1980), pp. 1103–1105. doi: [10.1143/PTP.64.1103](https://doi.org/10.1143/PTP.64.1103) (cited on page 10).
- [32] S. L. Glashow. “The Future of Elementary Particle Physics”. In: *NATO Sci. Ser. B* 61 (1980), p. 687. doi: [10.1007/978-1-4684-7197-7_15](https://doi.org/10.1007/978-1-4684-7197-7_15) (cited on page 10).
- [33] M. Gell-Mann, P. Ramond, and R. Slansky. “Complex Spinors and Unified Theories”. In: *Conf. Proc. C* 790927 (1979), pp. 315–321 (cited on page 10).
- [34] R. N. Mohapatra and G. Senjanović. “Neutrino Mass and Spontaneous Parity Nonconservation”. In: *Phys. Rev. Lett.* 44 (14 Apr. 1980), pp. 912–915. doi: [10.1103/PhysRevLett.44.912](https://doi.org/10.1103/PhysRevLett.44.912) (cited on page 10).
- [35] M. G. Aartsen et al. “eV-Scale Sterile Neutrino Search Using Eight Years of Atmospheric Muon Neutrino Data from the IceCube Neutrino Observatory”. In: *Phys. Rev. Lett.* 125.14 (2020), p. 141801. doi: [10.1103/PhysRevLett.125.141801](https://doi.org/10.1103/PhysRevLett.125.141801) (cited on page 10).
- [36] J.-L. Tastet, O. Ruchayskiy, and I. Timiryasov. “Reinterpreting the ATLAS bounds on heavy neutral leptons in a realistic neutrino oscillation model”. In: *JHEP* 12 (2021), p. 182. doi: [10.1007/JHEP12\(2021\)182](https://doi.org/10.1007/JHEP12(2021)182) (cited on page 10).
- [37] D. A. Bryman and R. Shrock. “Constraints on Sterile Neutrinos in the MeV to GeV Mass Range”. In: *Phys. Rev. D* 100 (2019), p. 073011. doi: [10.1103/PhysRevD.100.073011](https://doi.org/10.1103/PhysRevD.100.073011) (cited on pages 11, 12).
- [38] A. Aguilar-Arevalo et al. “Improved search for heavy neutrinos in the decay $\pi \rightarrow e \nu$ ”. In: *Phys. Rev. D* 97.7 (2018), p. 072012. doi: [10.1103/PhysRevD.97.072012](https://doi.org/10.1103/PhysRevD.97.072012) (cited on page 11).

- [39] G. Bellini et al. “New limits on heavy sterile neutrino mixing in B8 decay obtained with the Borexino detector”. In: *Phys. Rev. D* 88.7 (2013), p. 072010. doi: [10.1103/PhysRevD.88.072010](https://doi.org/10.1103/PhysRevD.88.072010) (cited on pages 11, 14).
- [40] D. Britton et al. “Improved search for massive neutrinos in $\pi^+ \rightarrow e + \nu$ decay”. In: *Physical Review D* 46 (1992) (cited on page 11).
- [41] C. J. Parkinson et al. “Search for heavy neutral lepton production at the NA62 experiment”. In: *PoS EPS-HEP2021* (2022), p. 686. doi: [10.22323/1.398.0686](https://doi.org/10.22323/1.398.0686) (cited on pages 11, 12).
- [42] K. Abe et al. “Search for heavy neutrinos with the T2K near detector ND280”. In: *Phys. Rev. D* 100.5 (2019), p. 052006. doi: [10.1103/PhysRevD.100.052006](https://doi.org/10.1103/PhysRevD.100.052006) (cited on pages 11, 12).
- [43] P. Abreu et al. “Search for neutral heavy leptons produced in Z decays”. In: *Z. Phys. C* 74 (1997). [Erratum: *Z.Phys.C* 75, 580 (1997)], pp. 57–71. doi: [10.1007/s002880050370](https://doi.org/10.1007/s002880050370) (cited on pages 11, 13).
- [44] R. Barouki, G. Marocco, and S. Sarkar. “Blast from the past II: Constraints on heavy neutral leptons from the BEBC WA66 beam dump experiment”. In: *SciPost Phys.* 13 (2022), p. 118. doi: [10.21468/SciPostPhys.13.5.118](https://doi.org/10.21468/SciPostPhys.13.5.118) (cited on pages 11–13).
- [45] F. Bergsma et al. “A Search for Decays of Heavy Neutrinos”. In: *Phys. Lett. B* 128 (1983). Ed. by J. Tran Thanh Van, p. 361. doi: [10.1016/0370-2693\(83\)90275-7](https://doi.org/10.1016/0370-2693(83)90275-7) (cited on page 11).
- [46] G. Aad et al. “Search for heavy neutral leptons in decays of W bosons produced in 13 TeV pp collisions using prompt and displaced signatures with the ATLAS detector”. In: *JHEP* 10 (2019), p. 265. doi: [10.1007/JHEP10\(2019\)265](https://doi.org/10.1007/JHEP10(2019)265) (cited on pages 11, 12).
- [47] G. Aad et al. “Search for Heavy Neutral Leptons in Decays of W Bosons Using a Dilepton Displaced Vertex in $\sqrt{s} = 13\text{TeV}$ pp Collisions with the ATLAS Detector”. In: *Phys. Rev. Lett.* 131 (6 Aug. 2023), p. 061803. doi: [10.1103/PhysRevLett.131.061803](https://doi.org/10.1103/PhysRevLett.131.061803) (cited on pages 11, 12).
- [48] A. M. Sirunyan et al. “Search for heavy neutral leptons in events with three charged leptons in proton-proton collisions at $\sqrt{s} = 13\text{ TeV}$ ”. In: *Phys. Rev. Lett.* 120.22 (2018), p. 221801. doi: [10.1103/PhysRevLett.120.221801](https://doi.org/10.1103/PhysRevLett.120.221801) (cited on pages 11, 12).
- [49] A. Tumasyan et al. “Search for long-lived heavy neutral leptons with displaced vertices in proton-proton collisions at $\sqrt{s}=13\text{ TeV}$ ”. In: *JHEP* 07 (2022), p. 081. doi: [10.1007/JHEP07\(2022\)081](https://doi.org/10.1007/JHEP07(2022)081) (cited on pages 11, 12).
- [50] A. Vaitaitis et al. “Search for neutral heavy leptons in a high-energy neutrino beam”. In: *Phys. Rev. Lett.* 83 (1999), pp. 4943–4946. doi: [10.1103/PhysRevLett.83.4943](https://doi.org/10.1103/PhysRevLett.83.4943) (cited on pages 11, 12).
- [51] E. Fernandez-Martinez et al. “Effective portals to heavy neutral leptons”. In: *JHEP* 09 (2023), p. 001. doi: [10.1007/JHEP09\(2023\)001](https://doi.org/10.1007/JHEP09(2023)001) (cited on pages 11–13).
- [52] G. Bernardi et al. “Search for Neutrino Decay”. In: *Phys. Lett. B* 166 (1986), pp. 479–483. doi: [10.1016/0370-2693\(86\)91602-3](https://doi.org/10.1016/0370-2693(86)91602-3) (cited on page 11).
- [53] S. Ito et al. “Search for heavy neutrinos in $\pi^+ \rightarrow \mu^+ \nu$ decay and status of lepton universality test in the PIENU experiment”. In: *JPS Conf. Proc.* 33 (2021). Ed. by N. Saito, pp. 011131-1–011131-6. doi: [10.7566/JPSCP.33.011131](https://doi.org/10.7566/JPSCP.33.011131) (cited on page 11).
- [54] A. V. Artamonov et al. “Search for heavy neutrinos in $K^+ \rightarrow \mu^+ \nu_H$ decays”. In: *Phys. Rev. D* 91.5 (2015). [Erratum: *Phys.Rev.D* 91, 059903 (2015)], p. 052001. doi: [10.1103/PhysRevD.91.052001](https://doi.org/10.1103/PhysRevD.91.052001) (cited on pages 11, 12).
- [55] P. Abratenko et al. “Search for Heavy Neutral Leptons in Electron-Positron and Neutral-Pion Final States with the MicroBooNE Detector”. In: *Phys. Rev. Lett.* 132.4 (2024), p. 041801. doi: [10.1103/PhysRevLett.132.041801](https://doi.org/10.1103/PhysRevLett.132.041801) (cited on pages 11, 12).
- [56] P. Astier et al. “Search for heavy neutrinos mixing with tau neutrinos”. In: *Phys. Lett. B* 506 (2001), pp. 27–38. doi: [10.1016/S0370-2693\(01\)00362-8](https://doi.org/10.1016/S0370-2693(01)00362-8) (cited on page 11).
- [57] J. Orloff, A. N. Rozanov, and C. Santoni. “Limits on the mixing of tau neutrino to heavy neutrinos”. In: *Phys. Lett. B* 550 (2002), pp. 8–15. doi: [10.1016/S0370-2693\(02\)02769-7](https://doi.org/10.1016/S0370-2693(02)02769-7) (cited on pages 12, 13).

- [58] I. Boiarska et al. “Blast from the past: constraints from the CHARM experiment on Heavy Neutral Leptons with tau mixing”. In: (July 2021) (cited on pages 12, 13).
- [59] A. Cooper-Sarkar et al. “Search for heavy neutrino decays in the BEBC beam dump experiment”. In: *Physics Letters B* 160.1 (1985), pp. 207–211. doi: [https://doi.org/10.1016/0370-2693\(85\)91493-5](https://doi.org/10.1016/0370-2693(85)91493-5) (cited on page 12).
- [60] B. Shuve and M. E. Peskin. “Revision of the LHCb Limit on Majorana Neutrinos”. In: *Phys. Rev. D* 94.11 (2016), p. 113007. doi: [10.1103/PhysRevD.94.113007](https://doi.org/10.1103/PhysRevD.94.113007) (cited on page 12).
- [61] R. Aaij et al. “Search for heavy neutral leptons in $W^+ \rightarrow \mu^+ \mu^\pm \text{jet}$ decays”. In: *Eur. Phys. J. C* 81.3 (2021), p. 248. doi: [10.1140/epjc/s10052-021-08973-5](https://doi.org/10.1140/epjc/s10052-021-08973-5) (cited on page 12).
- [62] R. Plestid. “Luminous solar neutrinos I: Dipole portals”. In: *Phys. Rev. D* 104 (2021), p. 075027. doi: [10.1103/PhysRevD.104.075027](https://doi.org/10.1103/PhysRevD.104.075027) (cited on pages 13, 14).
- [63] A. Osipowicz et al. “KATRIN: A Next generation tritium beta decay experiment with sub-eV sensitivity for the electron neutrino mass. Letter of intent”. In: (Sept. 2001) (cited on page 13).
- [64] S. Mertens et al. “A novel detector system for KATRIN to search for keV-scale sterile neutrinos”. In: *Journal of Physics G: Nuclear and Particle Physics* 46.6 (2019), p. 065203. doi: [10.1088/1361-6471/ab12fe](https://doi.org/10.1088/1361-6471/ab12fe) (cited on page 13).
- [65] M. Aker et al. “Search for keV-scale sterile neutrinos with the first KATRIN data”. In: *Eur. Phys. J. C* 83.8 (2023), p. 763. doi: [10.1140/epjc/s10052-023-11818-y](https://doi.org/10.1140/epjc/s10052-023-11818-y) (cited on page 13).
- [66] B. Abi et al. “Deep Underground Neutrino Experiment (DUNE), Far Detector Technical Design Report, Volume II: DUNE Physics”. In: (Feb. 2020) (cited on page 13).
- [67] S. Friedrich et al. “Limits on the Existence of sub-MeV Sterile Neutrinos from the Decay of ^7Be in Superconducting Quantum Sensors”. In: *Phys. Rev. Lett.* 126.2 (2021), p. 021803. doi: [10.1103/PhysRevLett.126.021803](https://doi.org/10.1103/PhysRevLett.126.021803) (cited on page 13).
- [68] C. Hagner et al. “Experimental search for the neutrino decay $\nu_3 + \nu_j + e^{++}e^-$ and limits on neutrino mixing”. English. In: 52.3 (1995), pp. 1343–1352. doi: [10.1103/PhysRevD.52.1343](https://doi.org/10.1103/PhysRevD.52.1343) (cited on page 13).
- [69] R. Plestid. “Luminous solar neutrinos II: Mass-mixing portals”. In: *Phys. Rev. D* 104 (2021). [Erratum: *Phys.Rev.D* 105, 099901 (2022)], p. 075028. doi: [10.1103/PhysRevD.104.075028](https://doi.org/10.1103/PhysRevD.104.075028) (cited on page 14).
- [70] P. Coloma et al. “Double-Cascade Events from New Physics in Icecube”. In: *Phys. Rev. Lett.* 119.20 (2017), p. 201804. doi: [10.1103/PhysRevLett.119.201804](https://doi.org/10.1103/PhysRevLett.119.201804) (cited on page 14).
- [71] P. Coloma. “Icecube/DeepCore tests for novel explanations of the MiniBooNE anomaly”. In: *Eur. Phys. J. C* 79.9 (2019), p. 748. doi: [10.1140/epjc/s10052-019-7256-8](https://doi.org/10.1140/epjc/s10052-019-7256-8) (cited on page 14).
- [72] M. Atkinson et al. “Heavy Neutrino Searches through Double-Bang Events at Super-Kamiokande, DUNE, and Hyper-Kamiokande”. In: *JHEP* 04 (2022), p. 174. doi: [10.1007/JHEP04\(2022\)174](https://doi.org/10.1007/JHEP04(2022)174) (cited on page 14).
- [73] P. Coloma et al. “GeV-scale neutrinos: interactions with mesons and DUNE sensitivity”. In: *Eur. Phys. J. C* 81.1 (2021), p. 78. doi: [10.1140/epjc/s10052-021-08861-y](https://doi.org/10.1140/epjc/s10052-021-08861-y) (cited on pages 14, 20).
- [74] M. Tanabashi et al. “Review of Particle Physics”. In: *Phys. Rev. D* 98 (3 Aug. 2018), p. 030001. doi: [10.1103/PhysRevD.98.030001](https://doi.org/10.1103/PhysRevD.98.030001) (cited on pages 15, 17).
- [75] M. Honda et al. “Atmospheric neutrino flux calculation using the NRLMSISE-00 atmospheric model”. In: *Phys. Rev. D* 92 (2 July 2015), p. 023004. doi: [10.1103/PhysRevD.92.023004](https://doi.org/10.1103/PhysRevD.92.023004) (cited on pages 15, 24).
- [76] A. Fedynitch et al. “Calculation of conventional and prompt lepton fluxes at very high energy”. In: *European Physical Journal Web of Conferences*. Vol. 99. European Physical Journal Web of Conferences. Aug. 2015, p. 08001. doi: [10.1051/epjconf/20159908001](https://doi.org/10.1051/epjconf/20159908001) (cited on page 16).
- [77] P. A. M. Dirac. “The Quantum Theory of the Emission and Absorption of Radiation”. In: *Proceedings of the Royal Society of London Series A* 114.767 (Mar. 1927), pp. 243–265. doi: [10.1098/rspa.1927.0039](https://doi.org/10.1098/rspa.1927.0039) (cited on page 16).
- [78] I. Esteban et al. “The fate of hints: updated global analysis of three-flavor neutrino oscillations”. In: *JHEP* 09 (2020), p. 178. doi: [10.1007/JHEP09\(2020\)178](https://doi.org/10.1007/JHEP09(2020)178) (cited on page 17).

- [79] A. Terliuk. “Measurement of atmospheric neutrino oscillations and search for sterile neutrino mixing with IceCube DeepCore”. PhD thesis. Berlin, Germany: Humboldt-Universität zu Berlin, Mathematisch-Naturwissenschaftliche Fakultät, 2018. doi: [10.18452/19304](https://doi.org/10.18452/19304) (cited on page 18).
- [80] J. A. Formaggio and G. P. Zeller. “From eV to EeV: Neutrino cross sections across energy scales”. In: *Rev. Mod. Phys.* 84 (3 Sept. 2012), pp. 1307–1341. doi: [10.1103/RevModPhys.84.1307](https://doi.org/10.1103/RevModPhys.84.1307) (cited on page 19).
- [81] R. Abbasi et al. “Measurement of atmospheric neutrino mixing with improved IceCube DeepCore calibration and data processing”. In: *Phys. Rev. D* 108 (1 July 2023), p. 012014. doi: [10.1103/PhysRevD.108.012014](https://doi.org/10.1103/PhysRevD.108.012014) (cited on pages 23, 30, 31, 34, 36).
- [82] C. Andreopoulos et al. “The GENIE Neutrino Monte Carlo Generator: Physics and User Manual”. In: (2015) (cited on pages 25, 35).
- [83] M. Glück, E. Reya, and A. Vogt. “Dynamical parton distributions revisited”. In: *The European Physical Journal C* 5 (Sept. 1998), pp. 461–470. doi: [10.1007/s100529800978](https://doi.org/10.1007/s100529800978) (cited on page 25).
- [84] A. Bodek and U. K. Yang. “Higher twist, $\xi(\omega)$ scaling, and effective LO PDFs for lepton scattering in the few GeV region”. In: *Journal of Physics G: Nuclear and Particle Physics* 29.8 (2003), p. 1899. doi: [10.1088/0954-3899/29/8/369](https://doi.org/10.1088/0954-3899/29/8/369) (cited on page 25).
- [85] J.-H. Koehne et al. “PROPOSAL: A tool for propagation of charged leptons”. In: *Computer Physics Communications* 184.9 (2013), pp. 2070–2090. doi: <https://doi.org/10.1016/j.cpc.2013.04.001> (cited on page 25).
- [86] S. Agostinelli et al. “Geant4—a simulation toolkit”. In: *Nucl. Instr. Meth. Phys. Res.* 506.3 (July 2003), pp. 250–303. doi: [10.1016/S0168-9002\(03\)01368-8](https://doi.org/10.1016/S0168-9002(03)01368-8) (cited on page 25).
- [87] L. Rädcl and C. Wiebusch. “Calculation of the Cherenkov light yield from low energetic secondary particles accompanying high-energy muons in ice and water with Geant4 simulations”. In: *Astroparticle Physics* 38 (Oct. 2012), pp. 53–67. doi: [10.1016/j.astropartphys.2012.09.008](https://doi.org/10.1016/j.astropartphys.2012.09.008) (cited on page 25).
- [88] Y. Becherini et al. “A parameterisation of single and multiple muons in the deep water or ice”. In: *Astroparticle Physics* 25.1 (2006), pp. 1–13. doi: <https://doi.org/10.1016/j.astropartphys.2005.10.005> (cited on page 25).
- [89] D. Heck et al. “CORSIKA: A Monte Carlo code to simulate extensive air showers”. In: (Feb. 1998) (cited on page 25).
- [90] T. K. Gaisser. “Spectrum of cosmic-ray nucleons, kaon production, and the atmospheric muon charge ratio”. In: *Astropart. Phys.* 35 (2012), pp. 801–806. doi: [10.1016/j.astropartphys.2012.02.010](https://doi.org/10.1016/j.astropartphys.2012.02.010) (cited on page 25).
- [91] R. Engel et al. “The hadronic interaction model Sibyll – past, present and future”. In: *EPJ Web Conf.* 145 (2017). Ed. by B. Pattison, p. 08001. doi: [10.1051/epjconf/201614508001](https://doi.org/10.1051/epjconf/201614508001) (cited on page 25).
- [92] C. Kopper et al. <https://github.com/claudiok/clsim> (cited on page 26).
- [93] D. Chirkin et al. “Photon Propagation using GPUs by the IceCube Neutrino Observatory”. In: *2019 15th International Conference on eScience (eScience)*. 2019, pp. 388–393. doi: [10.1109/eScience.2019.00050](https://doi.org/10.1109/eScience.2019.00050) (cited on page 26).
- [94] M. G. Aartsen et al. “Measurement of South Pole ice transparency with the IceCube LED calibration system”. In: *Nucl. Instrum. Meth. A* 711 (2013), pp. 73–89. doi: [10.1016/j.nima.2013.01.054](https://doi.org/10.1016/j.nima.2013.01.054) (cited on page 26).
- [95] G. Mie. “Beiträge zur Optik trüber Medien, speziell kolloidaler Metallösungen”. In: *Annalen der Physik* 330.3 (1908), pp. 377–445. doi: <https://doi.org/10.1002/andp.19083300302> (cited on page 26).
- [96] L. G. Henyey and J. L. Greenstein. “Diffuse radiation in the Galaxy.” In: *apj* 93 (Jan. 1941), pp. 70–83. doi: [10.1086/144246](https://doi.org/10.1086/144246) (cited on page 26).
- [97] S. Fiedlschuster. “The Effect of Hole Ice on the Propagation and Detection of Light in IceCube”. In: (Apr. 2019) (cited on page 26).
- [98] M. G. Aartsen et al. “In-situ calibration of the single-photoelectron charge response of the IceCube photomultiplier tubes”. In: *Journal of Instrumentation* 15.6 (June 2020), P06032. doi: [10.1088/1748-0221/15/06/P06032](https://doi.org/10.1088/1748-0221/15/06/P06032) (cited on page 27).

- [99] M. Larson. “Simulation and Identification of Non-Poissonian Noise Triggers in the IceCube Neutrino Detector”. Available at <https://ir.ua.edu/handle/123456789/1927>. MA thesis. University of Alabama, Tuscaloosa, AL, USA, 2013 (cited on page 27).
- [100] M. Larson. “A Search for Tau Neutrino Appearance with IceCube-DeepCore”. available at https://discoverycenter.nbi.ku.dk/teaching/thesis_page/mjlarson_thesis.pdf. PhD thesis. University of Copenhagen, Denmark, 2018 (cited on page 27).
- [101] E. Lohfink. “Testing nonstandard neutrino interaction parameters with IceCube-DeepCore”. PhD thesis. Mainz, Germany: Johannes Gutenberg-Universität Mainz, Fachbereich für Physik, Mathematik und Informatik, 2023. doi: <http://doi.org/10.25358/openscience-9288> (cited on page 27).
- [102] M. G. Aartsen et al. “The IceCube Neutrino Observatory: Instrumentation and Online Systems”. In: *JINST* 12.03 (2017), P03012. doi: [10.1088/1748-0221/12/03/P03012](https://doi.org/10.1088/1748-0221/12/03/P03012) (cited on page 28).
- [103] R. Abbasi et al. “The design and performance of IceCube DeepCore”. In: *Astropart. Phys.* 35.10 (2012), pp. 615–624. doi: [10.1016/j.astropartphys.2012.01.004](https://doi.org/10.1016/j.astropartphys.2012.01.004) (cited on page 28).
- [104] R. Abbasi et al. “The IceCube data acquisition system: Signal capture, digitization, and timestamping”. In: *Nuclear Instruments and Methods in Physics Research Section A: Accelerators, Spectrometers, Detectors and Associated Equipment* 601.3 (2009), pp. 294–316. doi: <https://doi.org/10.1016/j.nima.2009.01.001> (cited on page 28).
- [105] J. H. Friedman. “Stochastic gradient boosting”. In: *Computational Statistics & Data Analysis* 38 (2002), pp. 367–378 (cited on page 30).
- [106] R. Abbasi et al. “Low energy event reconstruction in IceCube DeepCore”. In: *Eur. Phys. J. C* 82.9 (2022), p. 807. doi: [10.1140/epjc/s10052-022-10721-2](https://doi.org/10.1140/epjc/s10052-022-10721-2) (cited on page 31).
- [107] S. Yu and J. Micallef. “Recent neutrino oscillation result with the IceCube experiment”. In: *38th International Cosmic Ray Conference*. July 2023 (cited on page 31).
- [108] S. Yu and on behalf of the IceCube collaboration. “Direction reconstruction using a CNN for GeV-scale neutrinos in IceCube”. In: *Journal of Instrumentation* 16.11 (Nov. 2021), p. C11001. doi: [10.1088/1748-0221/16/11/C11001](https://doi.org/10.1088/1748-0221/16/11/C11001) (cited on pages 31, 32).
- [109] J. Micallef. <https://github.com/jessimic/LowEnergyNeuralNetwork> (cited on page 31).
- [110] M. Huennefeld. “Deep Learning in Physics exemplified by the Reconstruction of Muon-Neutrino Events in IceCube”. In: *PoS ICRC2017* (2017), p. 1057. doi: [10.22323/1.301.1057](https://doi.org/10.22323/1.301.1057) (cited on page 31).
- [111] H. Dembinski et al. “Data-driven model of the cosmic-ray flux and mass composition from 10 GeV to 10^{11} GeV”. In: *PoS ICRC2017* (2017), p. 533. doi: [10.22323/1.301.0533](https://doi.org/10.22323/1.301.0533) (cited on page 34).
- [112] G. D. Barr et al. “Uncertainties in atmospheric neutrino fluxes”. In: *Phys. Rev. D* 74 (9 Nov. 2006), p. 094009. doi: [10.1103/PhysRevD.74.094009](https://doi.org/10.1103/PhysRevD.74.094009) (cited on page 34).
- [113] J. Evans et al. “Uncertainties in atmospheric muon-neutrino fluxes arising from cosmic-ray primaries”. In: *Phys. Rev. D* 95 (2 Jan. 2017), p. 023012. doi: [10.1103/PhysRevD.95.023012](https://doi.org/10.1103/PhysRevD.95.023012) (cited on page 34).
- [114] A. Fedynitch et al. <https://github.com/afedynitch/MCEq> (cited on page 34).
- [115] G. D. Barr et al. “Uncertainties in Atmospheric Neutrino Fluxes”. In: *Phys. Rev. D* 74 (2006), p. 094009. doi: [10.1103/PhysRevD.74.094009](https://doi.org/10.1103/PhysRevD.74.094009) (cited on pages 34, 35).
- [116] F. Riehn et al. “Hadronic interaction model sibyll 2.3d and extensive air showers”. In: *Phys. Rev. D* 102 (6 Sept. 2020), p. 063002. doi: [10.1103/PhysRevD.102.063002](https://doi.org/10.1103/PhysRevD.102.063002) (cited on page 34).
- [117] A. Cooper-Sarkar, P. Mertsch, and S. Sarkar. “The high energy neutrino cross-section in the Standard Model and its uncertainty”. In: *JHEP* 08 (2011), p. 042. doi: [10.1007/JHEP08\(2011\)042](https://doi.org/10.1007/JHEP08(2011)042) (cited on page 35).
- [118] Q. Wu et al. “A precise measurement of the muon neutrino–nucleon inclusive charged current cross section off an isoscalar target in the energy range $2.5 < E < 40$ GeV by NOMAD”. In: *Physics Letters B* 660.1 (2008), pp. 19–25. doi: <https://doi.org/10.1016/j.physletb.2007.12.027> (cited on page 36).
- [119] M. M. Tzanov. “Precise measurement of neutrino and anti-neutrino differential cross sections on iron”. PhD thesis. University of Pittsburgh, Pennsylvania, Jan. 2005 (cited on page 36).

- [120] W. G. Seligman. “A next-to-leading-order QCD analysis of neutrino-iron structure functions at the Tevatron”. PhD thesis. Columbia University, New York, Aug. 1997 (cited on page 36).
- [121] J. Feintzeig. “Searches for Point-like Sources of Astrophysical Neutrinos with the IceCube Neutrino Observatory”. PhD thesis. University of Wisconsin, Madison, Jan. 2014 (cited on page 36).
- [122] N. Kulacz. “In Situ Measurement of the IceCube DOM Efficiency Factor Using Atmospheric Minimum Ionizing Muons”. MA thesis. University of Alberta, 2019 (cited on page 36).
- [123] Rongen, Martin. “Measuring the optical properties of IceCube drill holes”. In: *EPJ Web of Conferences* 116 (2016), p. 06011. doi: [10.1051/epjconf/201611606011](https://doi.org/10.1051/epjconf/201611606011) (cited on page 36).
- [124] R. Abbasi et al. “In situ estimation of ice crystal properties at the South Pole using LED calibration data from the IceCube Neutrino Observatory”. In: *The Cryosphere* 18.1 (2024), pp. 75–102. doi: [10.5194/tc-18-75-2024](https://doi.org/10.5194/tc-18-75-2024) (cited on page 37).